



HAL
open science

A one-shot overlapping Schwarz method for component-based model reduction: application to nonlinear elasticity

Angelo Iollo, Giulia Sambataro, Tommaso Taddei

► To cite this version:

Angelo Iollo, Giulia Sambataro, Tommaso Taddei. A one-shot overlapping Schwarz method for component-based model reduction: application to nonlinear elasticity. *Computer Methods in Applied Mechanics and Engineering*, 2023, 404, pp.115786. 10.1016/j.cma.2022.115786 . hal-03910506v2

HAL Id: hal-03910506

<https://hal.science/hal-03910506v2>

Submitted on 28 Nov 2024

HAL is a multi-disciplinary open access archive for the deposit and dissemination of scientific research documents, whether they are published or not. The documents may come from teaching and research institutions in France or abroad, or from public or private research centers.

L'archive ouverte pluridisciplinaire **HAL**, est destinée au dépôt et à la diffusion de documents scientifiques de niveau recherche, publiés ou non, émanant des établissements d'enseignement et de recherche français ou étrangers, des laboratoires publics ou privés.

A one-shot overlapping Schwarz method for component-based model reduction: application to nonlinear elasticity.

Angelo Iollo¹, Giulia Sambataro¹, Tommaso Taddei¹

¹ *IMB, UMR 5251, Univ. Bordeaux, 33400 Talence, France, Inria Bordeaux Sud-Ouest, Team MEMPHIS, 33400 Talence, France,*
 angelo.iollo@inria.fr, giulia.sambataro@inria.fr,
 tommaso.taddei@inria.fr,

Abstract

We propose a component-based (CB) parametric model order reduction (pMOR) formulation for parameterized nonlinear elliptic partial differential equations (PDEs) based on overlapping subdomains. Our approach reads as a constrained optimization statement that penalizes the jump at the components' interfaces subject to the approximate satisfaction of the PDE in each local subdomain. Furthermore, the approach relies on the decomposition of the local states into a port component — associated with the solution on interior boundaries — and a bubble component that vanishes at ports: since the bubble components are uniquely determined by the solution value at the corresponding port, we can recast the constrained optimization statement into an unconstrained statement, which reads as a nonlinear least-squares problem and can be solved using the Gauss-Newton method. We present thorough numerical investigations for a two-dimensional neo-Hookean nonlinear mechanics problem to validate our method; we further discuss the well-posedness of the mathematical formulation and the *a priori* error analysis for linear coercive problems.

Keywords: parameterized partial differential equations; model order reduction; overlapping domain decomposition; alternating Schwarz method.

1 Introduction

1.1 Component-based model order reduction for nonlinear PDEs

Parametric model order reduction (pMOR, [25, 27, 47]) refers to a class of computational techniques that aim at constructing a low-dimensional surrogate (or reduced-order) model (ROM) for a given physical system, over a range of parameters. In the last few decades, pMOR techniques have received significant attention in science and engineering, to speed up parametric studies. For complex, large-scale systems with many parameters, methods that combine pMOR with domain decomposition (DD) methods are of paramount importance to deal with high-dimensional parameterizations and changes in domain topology. The aim of this work is to present a general DD pMOR strategy for linear and nonlinear steady partial differential equations (PDEs).

Standard (monolithic) pMOR techniques rely on high-fidelity (HF) solves at the training stage, which might be unaffordable for very large-scale problems; furthermore, they rely on the assumption that the solution field is defined over a parameter-independent domain or over a family of diffeomorphic domains: to address these issues, several authors have proposed component-based pMOR procedures (cf. [30] and the review [9]). During the offline stage, a library of *archetype components* is defined, and local reduced-order bases (ROBs) as well as local ROMs are built; then, during the online stage, local components are instantiated to form the global system and the global solution is estimated by coupling local ROMs.

CB-pMOR strategies consist of two distinct building blocks: (i) a rapid and reliable DD strategy for online global predictions, and (ii) a localized training strategy exclusively based on local solves for the construction of the local approximations. In this work, we focus exclusively on (i); we refer to [5, 54] and [28, section 8.1.7] for recent works on localized training for nonlinear elliptic PDEs.

We propose a general component-based pMOR procedure for steady PDEs based on overlapping subdomains, with a particular focus on second-order nonlinear elliptic PDEs. The key features of the approach are twofold: (i) a constrained optimization statement that penalizes the jump at the components' interfaces subject to the approximate (in a sense to be defined) satisfaction of the PDE in each deployed (instantiated) component; (ii) the decomposition of the local solutions into a *port component* — associated with the solution on interior boundaries (*ports*) — and a *bubble component* that vanishes at *ports*, to enable effective parallelization of the online solver.

arXiv:2207.05426v2 [math.NA] 21 Nov 2022

1.2 One-shot overlapping Schwarz method

We first introduce the formulation in the simplified case of two instantiated components Ω_1, Ω_2 (cf. Figure 1) — to simplify notation, we do not distinguish between archetype and instantiated components; in section 2, we present the formulation in the general setting. We denote by $\mathcal{X}_i \subset H^1(\Omega_i)$ a suitable Hilbert space in Ω_i ; we further define the *bubble space* $\mathcal{X}_{i,0} = \{v \in \mathcal{X}_i : v|_{\Gamma_i} = 0\}$ and the *port space* $\mathcal{U}_i = \{v \in \mathcal{X}_i : v|_{\Gamma_i} = 0\}$, for $i = 1, 2$. Then, we introduce the additive or multiplicative overlapping Schwarz (OS) iterations as

$$\begin{cases} \text{find } u_1^{(k)} \in \mathcal{X}_1 : \mathcal{G}_1(u_1^{(k)}, v) = 0 \quad \forall v \in \mathcal{X}_{1,0}, \quad u_1^{(k)}|_{\Gamma_1} = u_2^{(k-1)}; \\ \text{find } u_2^{(k)} \in \mathcal{X}_2 : \mathcal{G}_2(u_2^{(k)}, v) = 0 \quad \forall v \in \mathcal{X}_{2,0}, \quad u_2^{(k)}|_{\Gamma_2} = \begin{cases} u_1^{(k)}, \\ u_1^{(k-1)}, \end{cases} \end{cases} \quad (1)$$

for $k = 1, 2, \dots$. Here, $u_i^{(k)}$ denotes the state estimate at the k -th iteration in the i -th subdomain, while $\mathcal{G}_1, \mathcal{G}_2$ are the variational forms associated with the PDE of interest in Ω_1, Ω_2 . *Multiplicative* Schwarz iterations correspond to setting $u_2^{(k)}|_{\Gamma_2} = u_1^{(k)}$ in (1)₂, while *additive* Schwarz iterations correspond to setting $u_2^{(k)}|_{\Gamma_2} = u_1^{(k-1)}$. Convergence of the OS iterations to a limit state (u_1^*, u_2^*) implies that $\|u_1^* - u_2^*\|_{L^2(\Gamma_1 \cup \Gamma_2)} = 0$. We thus propose to consider the formulation

$$\min_{u_1 \in \mathcal{X}_1, u_2 \in \mathcal{X}_2} \|u_1 - u_2\|_{L^2(\Gamma_1 \cup \Gamma_2)} \quad \text{s.t.} \quad \mathcal{G}_i(u_i, v_i) = 0 \quad \forall v_i \in \mathcal{X}_{i,0}, \quad i = 1, 2. \quad (2)$$

Clearly, the pair (u_1^*, u_2^*) is a solution to (2); in section 4, we show that, provided that the overlapping size δ is strictly positive, the solution to (2) is unique and depends continuously on data for linear coercive problems. Note that, for linear problems, the solution to (2) can be computed directly without the need for an iterative scheme: we thus refer to our approach as to one-shot (OS) overlapping Schwarz (OS) method and we use the abbreviation OS2¹. From this point forward, we shall use the acronym OS to refer to the standard overlapping Schwarz method.

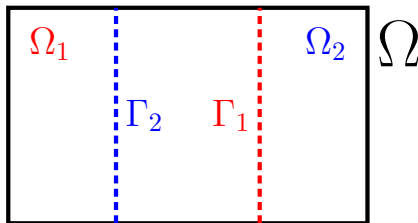


Figure 1: configuration considered for illustration in section 1 and for the analysis of the linear coercive problem in section 4.

In order to recast (2) into an unconstrained problem, we denote by u_1^p, u_2^p the port solutions, that is the restrictions of u_1 and u_2 to the corresponding ports; then, we introduce the extension operators $\mathbf{E}_i : \mathcal{U}_i \rightarrow \mathcal{X}_i$ and the local *port-to-bubble* solution maps $\mathbf{F}_i : \mathcal{U}_i \rightarrow \mathcal{X}_{i,0}$ such that, given $w \in \mathcal{U}_i$, we have $\mathcal{G}_i(\mathbf{F}_i(w) + \mathbf{E}_i w, v_i) = 0 \quad \forall v_i \in \mathcal{X}_{i,0}$, for $i = 1, 2$ — note that the *port-to-bubble* field is uniquely determined by the corresponding port solution. Then, we obtain the unconstrained OS2 statement:

$$\min_{u_1^p \in \mathcal{U}_1, u_2^p \in \mathcal{U}_2} \mathfrak{f}(u_1^p, u_2^p) := \|\mathbf{F}_1(u_1^p) + \mathbf{E}_1 u_1^p - \mathbf{F}_2(u_2^p) - \mathbf{E}_2 u_2^p\|_{L^2(\Gamma_1 \cup \Gamma_2)}^2. \quad (3)$$

The present derivation can be viewed as a *static condensation* of bubble degrees of freedom and is similar in scope to the approach in [30]. Following taxonomy from the optimization literature, we might view our approach as *black-box* — as opposed to *all-at-once* [26, section 1.1].

Note that (3) reads as a nonlinear least-squares problem: as in [10], we can thus resort to the Gauss-Newton method which exploits the underlying structure of the objective function to enable rapid convergence of the CB-ROM to the optimum.

Practical implementation of a CB-pMOR approach based on (2)-(3) requires to address three major tasks (i) (*data compression*) the minimization statement (3) is infinite-dimensional: we should thus drastically reduce the dimensionality of the port spaces $\mathcal{U}_1, \mathcal{U}_2$; (ii) (*reduction of local problems*) the local problems associated with the evaluation of the port-to-bubble maps are also infinite-dimensional: we should thus resort to standard (monolithic) MOR techniques to devise low-rank approximations of the bubble fields; (iii) (*hyper-reduction of the objective function*) evaluation of the objective function in (3) requires integration over the whole curve $\Gamma_1 \cup \Gamma_2$: we should thus devise a low-dimensional quadrature rule that requires evaluation of the local fields in

¹More rigorously, we should consider the acronym OSOS or (OS)²; however, we opted for OS2 to simplify the notation.

a moderate number of quadrature points. In this work, we propose specialized MOR strategies to address these three tasks: we resort to proper orthogonal decomposition (POD, [58]) based on the method of snapshots [52] to build low-dimensional port spaces; we rely on Galerkin ROMs (see, e.g., [25, 27, 47]) with hyper-reduction based on empirical quadrature/mesh sampling and weighting [22, 63]; finally, we consider two distinct approaches to speed up the computation of the objective function: the former is based on empirical quadrature, while the latter relies on the empirical interpolation method (EIM, [4]).

Exploiting the static condensation of the bubble degrees of freedom, we can interpret the OS2 ROM as a minimum residual formulation of the port (or interface) problem associated with the underlying PDE. We discuss this interpretation for linear coercive problems in section 4. We remark that, similarly to [38], our analysis exploits a variational interpretation of the Schwarz method.

The outline of the paper is as follows. In section 2, we present the variational OS2 formulation for general nonlinear PDEs in arbitrary geometries. In section 3, we discuss the construction of local approximation spaces, hyper-reduction of the local models and of the objective function. In section 4, we discuss the well-posedness of the OS2 statement for linear coercive problems and we present an *a priori* error analysis of the OS2 ROM; furthermore, we comment on the connection between OS and OS2 and we provide explicit convergence rates for two representative one-dimensional problems. In section 5, we investigate performance of our method for a nonlinear elasticity problem. Section 6 concludes the paper.

1.3 Relation to previous works

The aim of this work is to devise a CB-pMOR DD strategy for nonlinear PDEs: we emphasize the development of an effective solution strategy based on the Gauss-Newton method and on hyper-reduction of the objective function and of the local problems. The literature on DD for MOR and reduced-order model /full-order model (ROM-FOM) coupling is extremely vast: CB-pMOR strategies have been presented in [33, 30, 28, 31, 43, 46] and also recently reviewed in [9]; ROM/FOM coupling strategies have been proposed for a broad range of applications including compressible flows [16, 36, 39, 50] incompressible flows [2, 6, 59], and structural mechanics [17, 34, 49] — these methods do not distinguish between archetype and instantiated components and do not necessarily involve the training of a library of local ROMs. Recently, several authors have proposed to couple iterative Schwarz DD strategies with local non-intrusive ROMs based on neural network approximations [13, 37].

The OS2 statement shares several features with the minimization formulation first proposed in [19] in the DD literature, for coercive linear elliptic PDEs. OS2 is also tightly linked to the method proposed in [21] for the coupling of local and nonlocal diffusion models (see also [7]): as in [21], we interpret the OS2 statement as a control problem; while in [21] the controls are the nonlocal volume constraint and the local boundary condition, in this work the controls are the local solutions at ports. We also observe that the authors of [21] do not exploit the nonlinear least-square structure of the problem and rely on a quasi-Newton scheme to approximate the solution. We show that the choice of using the port solutions as control variables enables the definition of configuration-independent archetype components and is thus key for CB-pMOR.

Our approach is related to the Galerkin-free approach proposed in [8] and further developed in [6]. In [8, 6], the authors consider a HF model in the region of interest and rely on a low-dimensional expansion for the far-field; instead of projecting the equations in the far-field onto a low-dimensional test space, they simply rely on the objective function to compute the far-field solution coefficients (Galerkin-free). Exploiting notation introduced in the previous section, we can state the methods in [8, 6] as:

$$\min_{u_1 \in \mathcal{X}_1, w_2 \in \mathcal{Z}_2} \|u_1 - u_2\|_{L^2(\Omega_1 \cap \Omega_2)} \quad \text{s.t.} \quad \mathcal{G}_1(u_1, v_1) = 0 \quad \forall v_1 \in \mathcal{X}_{1,0},$$

where \mathcal{X}_1 denotes the HF space in Ω_1 and \mathcal{Z}_2 denotes the reduced-order space in Ω_2 . The approach presented in this work is more general, more robust and also leads to more efficient online calculations, at the price of a much more involved implementation.

Our approach is linked to the minimum residual formulation in [28]: the authors consider a minimization statement in which continuity of solution and fluxes is enforced as a constraint in the formulation, while the global dual residual enters directly in the objective function. The imposition of continuity in the objective function removes compatibility requirements at ports and allows the use of independent spaces in each archetype component; in particular, the use of an overlapping partition allows us to neither explicitly enforce continuity of the solution at ports nor to enforce continuity of normal fluxes. For highly-nonlinear PDEs, we found that this feature remarkably simplifies the implementation of our method and ultimately increases its flexibility.

Finally, the OS2 approach can be interpreted as an alternative to the partition-of-unity method (PUM, [1]) considered in [54]. Given local approximation spaces, PUM relies on the introduction of a partition of unity to define a global approximation space, and on Galerkin projection to devise the ROM for the deployed system. PUM has strong theoretical guarantees both in terms of approximation and in terms of quasi-optimality properties. Similarly to OS2, PUM requires efficient mesh interpolation to achieve online efficiency. The major difference between OS2 and PUM is that PUM relies on a global variational formulation based on a single

model: on the other hand, since in OS2 local models are independent of each other, OS2 can be used to couple different models in different regions of the domain.

2 Formulation

2.1 Preliminary definitions

We use the superscript $(\cdot)^a$ to indicate quantities and spaces defined for a given archetype component; we further denote by ℓ a generic element of the library \mathcal{L} of archetype components. We define the archetype components $\{\Omega_\ell^a\}_{\ell \in \mathcal{L}} \subset \mathbb{R}^d$; we denote by $\Gamma_\ell^{\text{a,dir}}$ the open subset of $\partial\Omega_\ell^a$ where we impose Dirichlet boundary conditions, and we denote by Γ_ℓ^a the portion of $\partial\Omega_\ell^a$ that lies inside the computational domain (“port”). For each archetype component $\ell \in \mathcal{L}$, we define the local discrete high-fidelity (HF) finite element (FE) space $\mathcal{X}_\ell^a \subset [H_{0,\Gamma_\ell^{\text{a,dir}}}^1(\Omega_\ell^a)]^D$ where D denotes the number of state variables, the bubble space $\mathcal{X}_{\ell,0}^a = \{v \in \mathcal{X}_\ell^a : v|_{\Gamma_\ell^a} = 0\}$, and the port space $\mathcal{U}_\ell^a = \{v|_{\Gamma_\ell^a} : v \in \mathcal{X}_\ell^a\} \subset [H^{1/2}(\Gamma_\ell^a)]^D$. We endow \mathcal{X}_ℓ^a with the inner product $(\cdot, \cdot)_\ell$ and the induced norm $\|\cdot\|_\ell = \sqrt{(\cdot, \cdot)_\ell}$, we define $N_\ell^a = \dim(\mathcal{X}_\ell^a)$, and the extension operator $\mathbf{E}_\ell^a : \mathcal{U}_\ell^a \rightarrow \mathcal{X}_\ell^a$ such that

$$(\mathbf{E}_\ell^a w, v)_\ell = 0 \quad \forall v \in \mathcal{X}_{\ell,0}^a, \quad \mathbf{E}_\ell^a w|_{\Gamma_\ell^a} = w, \quad \forall w \in \mathcal{U}_\ell^a. \quad (4)$$

We define the vector of local parameters μ_ℓ in the parameter region \mathcal{P}_ℓ , which include geometric and material parameters that identify the physical model in any instantiated component of type ℓ . We define the variational form $\mathcal{G}_\ell^a : \mathcal{X}_\ell^a \times \mathcal{X}_{\ell,0}^a \times \mathcal{P}_\ell \rightarrow \mathbb{R}$ such that

$$\mathcal{G}_\ell^a(w, v; \mu_\ell) = \sum_{k=1}^{N_\ell^e} \int_{\mathcal{D}_{\ell,k}} \eta_\ell^{\text{a,e}}(w, v; \mu_\ell) dx + \int_{\partial\mathcal{D}_{\ell,k}} \eta_\ell^{\text{a,f}}(w, v; \mu_\ell) dx \quad (5)$$

where $\{\mathcal{D}_{\ell,k}\}_{k=1}^{N_\ell^e}$ denote the elements of the FE mesh for the archetype component Ω_ℓ^a . Furthermore, for any $\ell \in \mathcal{L}$, we define the parametric mapping $\Phi_\ell^a : \Omega_\ell^a \times \mathcal{P}_\ell \rightarrow \mathbb{R}^d$ that describes the deformation of the archetype component ℓ for the parameter value $\mu_\ell \in \mathcal{P}_\ell$.

A physical system is uniquely described by a set of N_{dd} labels $\{\mathbf{L}_i\}_{i=1}^{N_{\text{dd}}} \subset \mathcal{L}$, and the set of parameters $\mu := (\mu_1, \dots, \mu_{N_{\text{dd}}}) \in \mathcal{P} := \bigotimes_{i=1}^{N_{\text{dd}}} \mathcal{P}_{\mathbf{L}_i}$. Given $\mu \in \mathcal{P}$, we define

- (i) the mappings $\{\Phi_i\}_{i=1}^{N_{\text{dd}}}$ such that $\Phi_i = \Phi_{\mathbf{L}_i}^a(\cdot; \mu_i)$ for $i = 1, \dots, N_{\text{dd}}$;
- (ii) the instantiated overlapping partition $\{\Omega_i = \Phi_i(\Omega_{\mathbf{L}_i}^a)\}_{i=1}^{N_{\text{dd}}}$, the global open domain $\Omega \subset \mathbb{R}^d$ such that $\bar{\Omega} = \bigcup_i \bar{\Omega}_i$, the ports $\Gamma_i = \Phi_i(\Gamma_{\mathbf{L}_i}^a)$ and the Dirichlet boundaries $\Gamma_i^{\text{dir}} = \Phi_i(\Gamma_{\mathbf{L}_i}^{\text{a,dir}})$, for $i = 1, \dots, N_{\text{dd}}$;
- (iii) the deployed FE full, bubble, and port spaces $\mathcal{X}_i = \{v \circ \Phi_i^{-1} : v \in \mathcal{X}_{\mathbf{L}_i}^a\}$, $\mathcal{X}_{i,0} = \{v \circ \Phi_i^{-1} : v \in \mathcal{X}_{\mathbf{L}_i,0}^a\}$, and $\mathcal{U}_i = \{v|_{\Gamma_i} : v \in \mathcal{X}_i\}$, for $i = 1, \dots, N_{\text{dd}}$;
- (iv) the extension operators $\mathbf{E}_i : \mathcal{U}_i \rightarrow \mathcal{X}_i$ such that $\mathbf{E}_i w = \mathbf{E}_{\mathbf{L}_i}^a(w \circ \Phi_i) \circ \Phi_i^{-1}$ for $i = 1, \dots, N_{\text{dd}}$;
- (v) the deployed variational forms $\mathcal{G}_i : \mathcal{X}_i \times \mathcal{X}_{i,0} \rightarrow \mathbb{R}$ such that

$$\mathcal{G}_i(w, v) = \mathcal{G}_{\mathbf{L}_i}^a(w \circ \Phi_i, v \circ \Phi_i; \mu_i). \quad (6)$$

Given $i = 1, \dots, N_{\text{dd}}$, we further define the set of neighboring elements $\text{Neigh}_i = \{j : \Omega_j \cap \Omega_i \neq \emptyset, j \neq i\}$, and the partition of Γ_i $\{\Gamma_{i,j} = \Gamma_i \cap \Omega_j : j \in \text{Neigh}_i\}$ — note that $\Gamma_{i,j} \neq \Gamma_{j,i}$.

Given the archetype mesh $\mathcal{T}_\ell^a = \left(\{x_{\ell,j}^{\text{a,v}}\}_{j=1}^{N_\ell^{\text{v}}}, \mathbf{T}_\ell\right)$, with nodes $\{x_{\ell,j}^{\text{a,v}}\}_{j=1}^{N_\ell^{\text{v}}}$, connectivity matrix \mathbf{T}_ℓ and elements $\{\mathcal{D}_{k,\ell}\}_{k=1}^{N_\ell^e}$, we denote by u a generic element of \mathcal{X}_ℓ and we denote by $\mathbf{u} \in \mathbb{R}^{DN_\ell^{\text{v}}}$ the corresponding FE vector associated with the Lagrangian basis of \mathcal{T}_ℓ^a , for all $\ell \in \mathcal{L}$. Following [57], we pursue a discretize-then-map treatment of parameterized geometries: given the mesh $\mathcal{T}_{\mathbf{L}_i}^a$, we state the local variational problems in the deformed mesh $\Phi_i(\mathcal{T}_{\mathbf{L}_i}^a) = \left(\{\Phi_i(x_{j,\mathbf{L}_i}^{\text{a,v}})\}_{j=1}^{N_{\mathbf{L}_i}^{\text{v}}}, \mathbf{T}_{\mathbf{L}_i}\right)$. In section 3.2, we discuss the hyper-reduced formulation of the local problems. Note that if $(\mathcal{T}_\ell^a, \mathbf{u})$ is associated with the element $u \in \mathcal{X}_\ell$, then $(\Phi_i(\mathcal{T}_{\mathbf{L}_i}^a), \mathbf{u})$ approximates $u \circ \Phi_i^{-1}$.

2.2 Model problem

We illustrate the many elements of the formulation for the two-dimensional (plane stress) nonlinear (neo-Hookean) elasticity problem considered in the numerical experiments. The problem shares the same geometric configuration with the problem studied in [32] for radioactive management applications. We consider the constitutive law for the first Piola Kirchhoff stress tensor

$$P(F(u)) = \lambda_2 (F(u) - F(u)^{-T}) + \lambda_1 \log(\det(F(u))) F(u)^{-T}. \quad (7a)$$

Here, $F(u) = \mathbb{1} + \nabla u$ is the deformation gradient associated with the displacement u , λ_1, λ_2 are the Lamé constants given by

$$\lambda_1 = \frac{E\nu}{1-\nu^2}, \quad \lambda_2 = \frac{E}{2(1+\nu)}, \quad (7b)$$

where E is the Young's modulus, and ν is the Poisson's ratio. We consider the domain $\Omega = (0, 1)^2$ depicted in Figure 2; we set $\nu = 0.3$ and we consider $E = E_k$ in ω_k for $k = 1, 2, 3$. We prescribe normal homogeneous Dirichlet conditions on the left and right boundaries; homogeneous Dirichlet conditions on the bottom boundary Γ_{btm} and the Neumann conditions:

$$P(F(u))\mathbf{n}|_{\Gamma_{\text{top}}} = g_{\text{top}} := \begin{bmatrix} 0 \\ -4x_1(1-x_1) \end{bmatrix}, \quad P(F(u))\mathbf{n}|_{\Gamma_{r,q}} = g_r := -s \begin{bmatrix} 0 \\ 1 \end{bmatrix}, \quad q = 1, \dots, Q_a \quad (7c)$$

with $s > 0$.

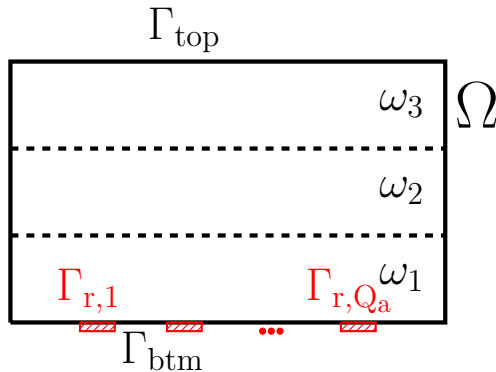


Figure 2: global system. Γ_{top} and $\Gamma_{r,1}, \dots, \Gamma_{r,Q_a}$ are associated with the stress conditions; the regions $\{\Gamma_{r,q}\}_q$ are of equal size $\ell_r > 0$, and the distance between consecutive regions is constant and equal to $d > \ell_r$.

The system of equations below summarizes the problem: we seek the solution $u : \Omega \rightarrow \mathbb{R}^2$ to the system

$$\begin{cases} -\nabla \cdot P(F(u)) = 0 & \text{in } \Omega \\ u \cdot \mathbf{n} = 0 & \text{on } \{0, 1\} \times (0, 1) \\ P(F(u))\mathbf{n} = g_r & \text{on } \Gamma_r \\ P(F(u))\mathbf{n} = g_{\text{top}} & \text{on } \Gamma_{\text{top}} \\ u = 0 & \text{on } \Gamma_{\text{btm}} = (0, 1) \times \{0\} \setminus \Gamma_r \end{cases} \quad (8)$$

where $\Gamma_r = \bigcup_{q=1}^{Q_a} \Gamma_{r,q}$. Our goal is to estimate the solution to (8) for any choice of the Young's moduli (E_1, E_2, E_3) associated with the regions $\omega_1, \omega_2, \omega_3$ in $[25, 30] \times [10, 20] \times [10, 20]$, any value of $s \in [0.4, 1]$ in (7c), and any $Q_a \in \{2, \dots, 7\}$. Note that variations of Q_a induce topological changes that prevent the application of standard monolithic techniques.

We introduce the library of components Ω_{int}^a and Ω_{ext}^a depicted in Figure 3; in Figure 4 we show examples of instantiated components and we identify the corresponding ports. We denote by $\delta > 0$ the size of the overlap. The mapping Φ_{int}^a associated with the internal component is a simple horizontal shift, while the mapping Φ_{ext}^a associated with the external component consists in a piecewise-linear map in the horizontal direction and the identity map in the vertical direction. The internal component is uniquely described by the vector of parameters $\mu_{\text{int}} = [E_1, s, x_{\text{shift}}]$ where x_{shift} denotes the magnitude of the horizontal shift; the external component is described by the vector of parameters $\mu_{\text{ext}} = [E_1, E_2, E_3, d_{\text{ext}}]$ with $d_{\text{ext}} = Q_a d - \delta$. Note that

the external archetype component (cf. Figure 3) corresponds to the choice $Q_a = Q_{\text{ref}}$ with $Q_{\text{ref}} = 5$. We then introduce the variational forms:

$$\begin{cases} \mathcal{G}_{\text{int}}^a(w, v; \mu_{\text{int}}) = \int_{\Omega_{\text{int}}^a} \eta_{\text{int}}^{\text{a,e}}(w, v; \mu_{\text{int}}) dx + \int_{\Gamma_{\text{r}}^a} \eta_{\text{int}}^{\text{a,f}}(w, v; \mu_{\text{int}}) dx, \\ \mathcal{G}_{\text{ext}}^a(w, v; \mu_{\text{ext}}) = \int_{\Omega_{\text{ext}}^a} \eta_{\text{ext}}^{\text{a,e}}(w, v; \mu_{\text{ext}}) dx + \int_{\Gamma_{\text{top}}^a} \eta_{\text{ext}}^{\text{a,f}}(w, v; \mu_{\text{ext}}) dx. \end{cases} \quad (9a)$$

Explicit expressions of $\eta_{\ell}^{\text{a,e}}$ and $\eta_{\ell}^{\text{a,f}}$ can be obtained by resorting to change-of-variable formulas: given the mapping Φ , we denote by $\nabla_{\Phi} = \nabla \Phi^{-T} \nabla$ the corresponding ‘‘mapped’’ gradient and we define $\nabla_{s,\Phi} = \frac{1}{2} (\nabla_{\Phi} + \nabla_{\Phi}^T)$ and $F_{\Phi} = \mathbb{1} + \nabla_{\Phi}$. Then, we have (we omit dependence on the parameter to shorten notation)

$$\begin{aligned} \eta_{\text{int}}^{\text{a,e}}(w, v) &= \eta_{\text{ext}}^{\text{a,e}}(w, v) = P(F_{\Phi}(w)) : \nabla_{s,\Phi} v \det(\nabla \Phi), \\ \eta_{\text{int}}^{\text{a,f}}(w, v) &= v \cdot (g_{\text{r}} \circ \Phi) \|\nabla \Phi \hat{\mathbf{t}}\|_2, \quad \eta_{\text{ext}}^{\text{a,f}}(w, v) = v \cdot (g_{\text{top}} \circ \Phi) \|\nabla \Phi \hat{\mathbf{t}}\|_2, \end{aligned} \quad (9b)$$

where $\hat{\mathbf{t}}$ denotes the tangent vector to the surface.

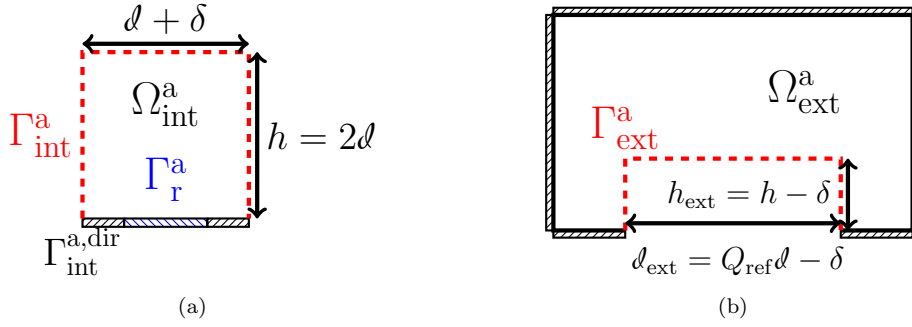


Figure 3: geometrical configuration. Archetype components. ($Q_{\text{ref}} = 5$).

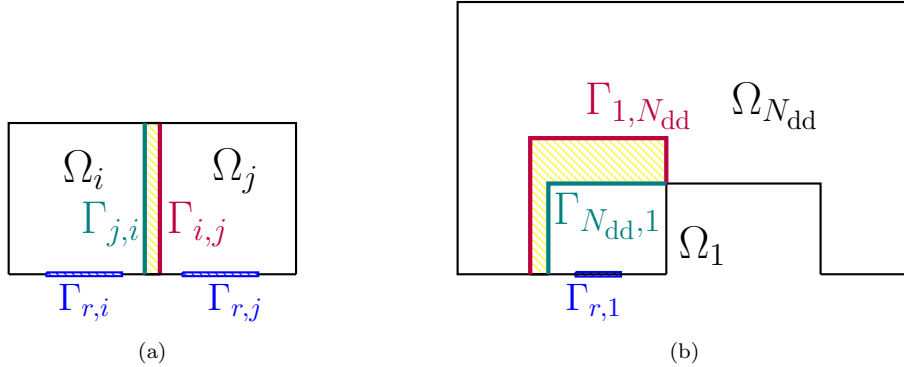


Figure 4: geometrical configuration. Examples of deployed components. (a): $i, j = 1, \dots, Q_a$, (b): $i = 1, j = N_{\text{dd}} = Q_a + 1$. The overlap area is marked in yellow.

2.3 Hybridized statement

2.3.1 High-dimensional formulation

We generalize below the OS2 statement introduced in section 1. Given the set of parameters $\mu = (\mu_1, \dots, \mu_{N_{\text{dd}}}) \in \mathcal{P} = \bigotimes_{i=1}^{N_{\text{dd}}} \mathcal{P}_{L_i}$, we propose the CB full-order model: find $u^{\text{hf}} = (u_1^{\text{hf}}, \dots, u_{N_{\text{dd}}}^{\text{hf}}) \in \mathcal{X} := \bigotimes_{i=1}^{N_{\text{dd}}} \mathcal{X}_i$ to minimize

$$\min_{u \in \mathcal{X}} \frac{1}{2} \sum_{i=1}^{N_{\text{dd}}} \sum_{j \in \text{Neigh}_i} \|u_i - u_j\|_{L^2(\Gamma_{i,j})}^2 \quad \text{s.t.} \quad \mathcal{G}_i(u_i, v_i) = 0 \quad \forall v_i \in \mathcal{X}_{i,0}, \quad i = 1, \dots, N_{\text{dd}}. \quad (10)$$

Note that (10) reduces to (2) for the case of two overlapping components.

To derive the hybridized formulation, we define the port-to-bubble maps $\mathbf{F}_i : \mathcal{U}_i \rightarrow \mathcal{X}_{i,0}$ such that, given $w \in \mathcal{U}_i$,

$$\mathcal{G}_i(\mathbf{F}_i(w) + \mathbf{E}_i w, v) = 0 \quad \forall v \in \mathcal{X}_{i,0}. \quad (11a)$$

Note that (11a) corresponds to the FE solution to a localized PDE problem with datum w on Γ_i . Then, we rewrite (10) as the unconstrained least-square problem: find $u^{\text{hf,p}} = (u_1^{\text{hf,p}}, \dots, u_{N_{\text{dd}}}^{\text{hf,p}}) \in \mathcal{U} := \bigotimes_{i=1}^{N_{\text{dd}}} \mathcal{U}_i$ to minimize

$$\min_{u^{\text{p}} \in \mathcal{U}} \frac{1}{2} \sum_{i=1}^{N_{\text{dd}}} \sum_{j \in \text{Neigh}_i} \|u_i^{\text{p}} - \mathbf{E}_j u_j^{\text{p}} - \mathbf{F}_j(u_j^{\text{p}})\|_{L^2(\Gamma_{i,j})}^2. \quad (11b)$$

Minimization problem (11b) reads as a nonlinear least-square problem; in the following we devise a low-dimensional reduced-order approximation of (11b) based on Galerkin projection of the port-to-bubble maps.

2.3.2 Reduced-order formulation

For all $\ell \in \mathcal{L}$, we introduce the low-dimensional archetype bubble and port spaces $\mathcal{Z}_\ell^{\text{a,b}} \subset \mathcal{X}_{\ell,0}$, $\mathcal{Z}_\ell^{\text{a,p}} \subset \mathcal{U}_\ell$ and the extended port spaces $\mathcal{W}_\ell^{\text{a,p}} = \{\mathbf{E}_\ell \zeta : \zeta \in \mathcal{Z}_\ell^{\text{a,p}}\} \subset \mathcal{X}_\ell$; we denote by n and m the dimensions of the bubble and port spaces, respectively; for simplicity, we assume that the dimension of the spaces is the same for all archetype components. We also define the archetype ROBs $Z_\ell^{\text{a,b}} : \mathbb{R}^n \rightarrow \mathcal{Z}_\ell^{\text{a,b}}$ and $W_\ell^{\text{a,b}} : \mathbb{R}^m \rightarrow \mathcal{W}_\ell^{\text{a,b}}$. Given the deployed system, we introduce the instantiated (or deployed) bubble and port spaces $\mathcal{Z}_i^{\text{b}} = \{\zeta \circ \Phi_i^{-1} : \zeta \in \mathcal{Z}_\ell^{\text{a,b}}\}$ and $\mathcal{W}_i^{\text{p}} = \{\zeta \circ \Phi_i^{-1} : \zeta \in \mathcal{W}_\ell^{\text{a,p}}\}$ with ROBs $Z_i^{\text{b}} = [\zeta_{i,1}^{\text{b}}, \dots, \zeta_{i,n}^{\text{b}}] : \mathbb{R}^n \rightarrow \mathcal{Z}_i^{\text{b}}$ and $W_i^{\text{p}} = [\psi_{i,1}^{\text{p}}, \dots, \psi_{i,m}^{\text{p}}] : \mathbb{R}^m \rightarrow \mathcal{W}_i^{\text{p}}$, respectively. Then, we define the ansatz:

$$\widehat{u}_i(\widehat{\alpha}_i, \widehat{\beta}_i) = Z_i^{\text{b}} \widehat{\alpha}_i + W_i^{\text{p}} \widehat{\beta}_i, \quad i = 1, \dots, N_{\text{dd}}. \quad (12)$$

We observe that $\widehat{u}_i^{\text{b}} = Z_i^{\text{b}} \widehat{\alpha}_i$ should approximate the bubble field $u|_{\Omega_i} - \mathbf{E}_i(u|_{\Gamma_i})$, while $\widehat{u}_i^{\text{p}} = W_i^{\text{p}} \widehat{\beta}_i$ is an approximation of the (extended) port field $\mathbf{E}_i(u|_{\Gamma_i})$: we refer to \widehat{u}_i^{b} , \widehat{u}_i^{p} as to the bubble and port estimates of the solution field in the i -th component.

To obtain the low-dimensional formulation, we introduce the local residuals² (cf. (5), (6) and (9))

$$\widehat{\mathbf{R}}_i^{\text{hf}} : \mathbb{R}^n \times \mathbb{R}^m \rightarrow \mathbb{R}^n \quad \text{s.t.} \quad \left(\widehat{\mathbf{R}}_i^{\text{hf}}(\alpha_i, \beta_i) \right)_j = \mathcal{G}_i(\widehat{u}_i(\alpha_i, \beta_i), \zeta_{i,j}^{\text{b}}), \quad i = 1, \dots, N_{\text{dd}}, \quad j = 1, \dots, n, \quad (13a)$$

and the approximate port-to-bubble maps $\widehat{\mathbf{F}}_i^{\text{hf}} : \mathbb{R}^m \rightarrow \mathbb{R}^n$ such that $\widehat{\mathbf{R}}_i^{\text{hf}}(\widehat{\mathbf{F}}_i^{\text{hf}}(\beta_i), \beta_i) = \mathbf{0}$. Computation of the port-to-bubble maps $\{\widehat{\mathbf{F}}_i^{\text{hf}}\}_i$ is expensive due to the need to integrate over the whole computational mesh. We thus replace the residuals $\{\widehat{\mathbf{R}}_i^{\text{hf}}\}_i$ with the empirical quadrature (EQ) approximations $\{\widehat{\mathbf{R}}_i^{\text{eq}}\}_i$ and we define the hyper-reduced port-to-bubble maps $\widehat{\mathbf{F}}_i^{\text{eq}} : \mathbb{R}^m \rightarrow \mathbb{R}^n$ such that

$$\widehat{\mathbf{R}}_i^{\text{eq}}(\widehat{\mathbf{F}}_i^{\text{eq}}(\beta_i), \beta_i) = \mathbf{0}. \quad (13b)$$

We discuss in section 3.2 the hyper-reduction strategy employed to construct the approximate residuals $\widehat{\mathbf{R}}_i^{\text{eq}}$; here, we observe that the gradient of the port-to-bubble map can be obtained by differentiating (13b):

$$\nabla \widehat{\mathbf{F}}_i^{\text{eq}}(\beta_i) = - \left(\partial_{\alpha_i} \widehat{\mathbf{R}}_i^{\text{eq}} \right)^{-1} \partial_{\beta_i} \widehat{\mathbf{R}}_i^{\text{eq}} \Big|_{(\alpha_i, \beta_i) = (\widehat{\mathbf{F}}_i^{\text{eq}}(\beta_i), \beta_i)} \quad (13c)$$

We remark that the existence and well-posedness of the port-to-bubble maps (13b) is conditioned to the existence of solutions to the nonlinear systems of equations $\widehat{\mathbf{R}}_i^{\text{hf}} = \mathbf{0}$ and to the fact that $\partial_{\alpha_i} \widehat{\mathbf{R}}_i^{\text{hf}}$ is non-singular at the optimum. It thus depends on the particular problem of interest, and might also depend on the overlapping partition considered and on the reduced-order approximation spaces.

We now focus on the objective function. We observe that

$$\begin{aligned} & \frac{1}{2} \sum_{i=1}^{N_{\text{dd}}} \sum_{j \in \text{Neigh}_i} \int_{\Gamma_{i,j}} \|\widehat{u}_i(x) - \widehat{u}_j(x)\|_2^2 dx \\ &= \frac{1}{2} \sum_{i=1}^{N_{\text{dd}}} \int_{\Gamma_i} \left(\sum_{j \in \text{Neigh}_i : x \in \Omega_j} \|\widehat{u}_i(x) - \widehat{u}_j(x)\|_2^2 \right) dx \\ &= \frac{1}{2} \sum_{i=1}^{N_{\text{dd}}} \int_{\Gamma_i^{\text{a}}} \left(\sum_{j \in \text{Neigh}_i : \Phi_i(\widehat{x}) \in \Omega_j} \|\widehat{u}_i(\Phi_i(\widehat{x})) - \widehat{u}_j(\Phi_i(\widehat{x}))\|_2^2 \right) J_i^{\text{bnd}}(\widehat{x}) d\widehat{x} \end{aligned}$$

²The superscript ^{hf} encodes the fact that the local residuals are computed using the HF mesh.

where $J_i^{\text{bnd}} = \|\det(\nabla\Phi_i)\nabla\Phi_i^{-T}\mathbf{n}_{L_i}^a\|_2$ and \mathbf{n}_ℓ^a is the outward normal to Γ_ℓ^a . Note that in the last identity we used the Nanson formula; furthermore, to shorten notation, we omitted dependence of $\widehat{u}_i, \widehat{u}_j$ on bubble and port coefficients (cf. (12)). We introduce the HF quadrature rules $\{(x_{\ell,q}^p, \rho_{\ell,q}^p)\}_{q=1}^{N_\ell^p}$ on the archetype ports Γ_ℓ^a for $\ell \in \mathcal{L}$; then, we have

$$\frac{1}{2} \sum_{i=1}^{N_{\text{dd}}} \sum_{j \in \text{Neigh}_i} \int_{\Gamma_{i,j}} \|\widehat{u}_i(\boldsymbol{\alpha}_i, \boldsymbol{\beta}_i) - \widehat{u}_j(\boldsymbol{\alpha}_j, \boldsymbol{\beta}_j)\|_2^2 dx \approx \frac{1}{2} \sum_{i=1}^{N_{\text{dd}}} \boldsymbol{\rho}_{L_i}^p \cdot \boldsymbol{\eta}_i^p(\boldsymbol{\alpha}, \boldsymbol{\beta}) \quad (14a)$$

where $\boldsymbol{\alpha} = [\boldsymbol{\alpha}_1, \dots, \boldsymbol{\alpha}_{N_{\text{dd}}}] \in \mathbb{R}^N$ with $N := nN_{\text{dd}}$, $\boldsymbol{\beta} = [\boldsymbol{\beta}_1, \dots, \boldsymbol{\beta}_{N_{\text{dd}}}] \in \mathbb{R}^M$, and

$$\boldsymbol{\eta}_i^p(\boldsymbol{\alpha}, \boldsymbol{\beta}) = \begin{bmatrix} \eta_i^p(\Phi_i(x_{\ell,1}^p); \boldsymbol{\alpha}, \boldsymbol{\beta}) \\ \vdots \\ \eta_i^p(\Phi_i(x_{\ell,N_\ell^p}^p); \boldsymbol{\alpha}, \boldsymbol{\beta}) \end{bmatrix} \quad (14b)$$

with

$$\eta_i^p(x; \boldsymbol{\alpha}, \boldsymbol{\beta}) = \left(\sum_{j \in \text{Neigh}_i: x \in \Omega_j} \|\widehat{u}_i(x; \boldsymbol{\alpha}_i, \boldsymbol{\beta}_i) - \widehat{u}_j(x; \boldsymbol{\alpha}_j, \boldsymbol{\beta}_j)\|_2^2 \right) J_i^{\text{bnd}}(\Phi_i^{-1}(x)), \quad (14c)$$

for $i = 1, \dots, N_{\text{dd}}$.

Evaluation of (14) is expensive due to the need to integrate over the port boundaries $\bigcup_{i=1}^{N_{\text{dd}}} \bigcup_{j \in \text{Neigh}_i} \Gamma_{i,j}$; we should thus replace the HF quadrature vectors $\{\boldsymbol{\rho}_\ell^p\}_{\ell \in \mathcal{L}}$ with sparse EQ vectors $\{\boldsymbol{\rho}_\ell^{\text{p,eq}}\}_{\ell \in \mathcal{L}}$. In conclusion, we obtain the discrete OS2 formulation: find $\widehat{\boldsymbol{\beta}} = [\widehat{\boldsymbol{\beta}}_1, \dots, \widehat{\boldsymbol{\beta}}_{N_{\text{dd}}}] \in \mathbb{R}^M$ such that

$$\widehat{\boldsymbol{\beta}} \in \arg \min_{\boldsymbol{\beta} \in \mathbb{R}^M} f^{\text{eq}}(\boldsymbol{\beta}) = \mathfrak{F}(\widehat{\mathbf{F}}^{\text{eq}}(\boldsymbol{\beta}), \boldsymbol{\beta}, \{\boldsymbol{\rho}_\ell^{\text{p,eq}}\}_{\ell \in \mathcal{L}}) \quad (15a)$$

where $\widehat{\mathbf{F}}^{\text{eq}}: \mathbb{R}^M \rightarrow \mathbb{R}^N$ is the full port-to-bubble map such that $\widehat{\mathbf{F}}^{\text{eq}}(\boldsymbol{\beta}) = [\widehat{\mathbf{F}}_1^{\text{eq}}(\boldsymbol{\beta}_1), \dots, \widehat{\mathbf{F}}_{N_{\text{dd}}}^{\text{eq}}(\boldsymbol{\beta}_{N_{\text{dd}}})]^T$, and

$$\mathfrak{F}(\boldsymbol{\alpha}, \boldsymbol{\beta}, \{\boldsymbol{\rho}_\ell^{\text{p,eq}}\}_{\ell \in \mathcal{L}}) = \frac{1}{2} \sum_{i=1}^{N_{\text{dd}}} \boldsymbol{\rho}_{L_i}^{\text{p,eq}} \cdot \boldsymbol{\eta}_i^p(\boldsymbol{\alpha}, \boldsymbol{\beta}). \quad (15b)$$

If we denote by Q the total number of quadrature points with repetitions times the number of state variables D ,

$$Q := D \left(\sum_{i=1}^{N_{\text{dd}}} \sum_{q=1}^{N_{L_i}^p} \text{card} \{j : \Phi_i(x_{L_i,q}^p) \in \Omega_j\} H(\rho_{L_i,q}^{\text{p,eq}}) \right), \quad \text{with } H(x) = \begin{cases} 1 & \text{if } x > 0 \\ 0 & \text{otherwise} \end{cases} \quad (15c)$$

we find that there exist $\mathbf{P} \in \mathbb{R}^{Q \times N}$ and $\mathbf{Q} \in \mathbb{R}^{Q \times M}$ such that

$$f^{\text{eq}}(\boldsymbol{\beta}) = \frac{1}{2} \|\mathbf{r}^{\text{eq}}(\boldsymbol{\beta})\|_2^2, \quad \text{where } \mathbf{r}^{\text{eq}}(\boldsymbol{\beta}) = \mathbf{P} \widehat{\mathbf{F}}^{\text{eq}}(\boldsymbol{\beta}) + \mathbf{Q}\boldsymbol{\beta}. \quad (15d)$$

2.4 Discussion

The remarks below provide a number of comments on the OS2 statement introduced in the previous section.

Remark 2.1. Algebraic representation of the local ROB. Exploiting notation introduced at the end of section 2.1, the archetype bubble ROB $Z_\ell^{\text{a,b}}: \mathbb{R}^n \rightarrow \mathcal{Z}_\ell^{\text{a,b}}$ admits the algebraic representation $Z_\ell^{\text{a,b}}: \boldsymbol{\alpha} \in \mathbb{R}^n \mapsto (\mathcal{J}_\ell^{\text{a}}, \mathbf{Z}_\ell^{\text{b}} \boldsymbol{\alpha})$ for some $\mathbf{Z}_\ell^{\text{b}} \in \mathbb{R}^{N_\ell^{\text{a}} \times n}$, while the deployed operators can be stated as $Z_i^{\text{b}}: \boldsymbol{\alpha} \in \mathbb{R}^n \mapsto (\Phi_i(\mathcal{J}_{L_i}^{\text{a}}, \mathbf{Z}_{L_i}^{\text{b}} \boldsymbol{\alpha}))$, for $i = 1, \dots, N_{\text{dd}}$. Note that by virtue of the correspondence between archetype and deployed spaces, we do not have to explicitly instantiate — and then store — the bubble ROB for each configuration. The same applies for the port bases.

Remark 2.2. Extension to non-homogeneous Dirichlet conditions. The OS2 formulation can readily deal with non-homogeneous Dirichlet boundary conditions. Towards this end, for $i = 1, \dots, N_{\text{dd}}$, given the Dirichlet datum $g_i^{\text{dir}}: \Gamma_i^{\text{dir}} \rightarrow \mathbb{R}^D$, we introduce the lift u_i^{dir} such that $u_i^{\text{dir}}|_{\Gamma_i^{\text{dir}}} = g_i^{\text{dir}}$, and the ansatz

$$\widehat{u}_i(\widehat{\boldsymbol{\alpha}}_i, \widehat{\boldsymbol{\beta}}_i) = u_i^{\text{dir}} + Z_i^{\text{b}} \widehat{\boldsymbol{\alpha}}_i + W_i^{\text{p}} \widehat{\boldsymbol{\beta}}_i, \quad i = 1, \dots, N_{\text{dd}}.$$

Here, $\widehat{u}_i^{\text{b}} = Z_i^{\text{b}} \widehat{\boldsymbol{\alpha}}_i$ should approximate the bubble field $u|_{\Omega_i} - \mathbf{E}_i((u - u_i^{\text{dir}})|_{\Gamma_i}) - u_i^{\text{dir}}$, while $\widehat{u}_i^{\text{p}} = W_i^{\text{p}} \widehat{\boldsymbol{\beta}}_i$ is an approximation of the (extended) port field $\mathbf{E}_i((u - u_i^{\text{dir}})|_{\Gamma_i})$. Then, we can proceed as before to derive the reduced port-to-bubble maps and the low-dimensional OS2 formulation. We refer to [24] for a thorough discussion on the imposition of Dirichlet boundary conditions in Galerkin ROMs.

Remark 2.3. Computation of the matrices \mathbf{P}, \mathbf{Q} . The matrices \mathbf{P}, \mathbf{Q} depend on the configuration of interest but are independent of the port coefficients β : they can thus be defined after having instantiated the system and before solving the optimization problem. Since the port quadrature points $\{\Phi_i(x_{L_i,q}^{\mathbf{P}})\}_{i,q}$ are configuration-dependent, we should resort to mesh interpolation to assemble the matrices \mathbf{P} and \mathbf{Q} . In this work, we rely on structured meshes in the archetype components that enable logarithmic-in- N_ℓ^y FE interpolations.

Remark 2.4. Hyper-reduction. As required in CB-pMOR, hyper-reduction should be defined at the component level and is then translated to the deployed system using the mappings $\{\Phi_i\}_i$. From an algorithmic standpoint, an archetype component $\ell \in \mathcal{L}$ should be interpreted as a complex data structure that comprises (i) bubble and port ROB; (ii) the approximate residual $\widehat{\mathbf{R}}_\ell^{\text{eq}}$ that enables effective computations of port-to-bubble maps; (iii) the port quadrature rule $\rho_\ell^{\text{p},\text{eq}}$ associated with the approximate objective function (15a); and (iv) a (structured) mesh structure for which efficient (i.e., logarithmic-in- N_ℓ^y) interpolation procedures are available for the computation of the matrices \mathbf{P}, \mathbf{Q} .

2.5 Solution to the OS2 minimization problem

In view of the description of the numerical solution to (15), we observe that the Jacobian of the global port-to-bubble map $\widehat{\mathbf{F}}^{\text{eq}} : \mathbb{R}^M \rightarrow \mathbb{R}^N$ is block-diagonal (cf. (13c)):

$$\widehat{\mathbf{J}}_{\mathbf{F}}^{\text{eq}}(\beta) = \text{diag} \left[\widehat{\mathbf{J}}_{\mathbf{F}_1}^{\text{eq}}(\beta_1), \dots, \widehat{\mathbf{J}}_{\mathbf{F}_{N_{\text{dd}}}}^{\text{eq}}(\beta_{N_{\text{dd}}}) \right], \quad \widehat{\mathbf{J}}_{\mathbf{F}_i}^{\text{eq}}(\beta_i) := - \left(\partial_{\alpha_i} \widehat{\mathbf{R}}_i^{\text{eq}} \right)^{-1} \partial_{\beta_i} \widehat{\mathbf{R}}_i^{\text{eq}} \Big|_{(\alpha_i, \beta_i) = (\widehat{\mathbf{F}}_i^{\text{eq}}(\beta_i), \beta_i)}. \quad (16a)$$

Then, we observe that

$$\nabla_{\mathbf{r}}^{\text{eq}} = \mathbf{P} \widehat{\mathbf{J}}_{\mathbf{F}}^{\text{eq}} + \mathbf{Q}, \quad \nabla_{\mathbf{f}}^{\text{eq}} = \left(\mathbf{P} \widehat{\mathbf{J}}_{\mathbf{F}}^{\text{eq}} + \mathbf{Q} \right)^T \mathbf{r}^{\text{eq}}. \quad (16b)$$

If $N_{\text{dd}} \gg m$ (as in the cases considered e.g. in [30, 43]), the Jacobian $\widehat{\mathbf{J}}_{\mathbf{F}}^{\text{eq}}$ is highly sparse; note that explicit assembly of the local Jacobians requires to solve m linear systems of size n , while matrix-vector multiplications $\widehat{\mathbf{J}}_{\mathbf{F}}^{\text{eq}} \mathbf{v}$ and $\mathbf{v}^T \widehat{\mathbf{J}}_{\mathbf{F}}^{\text{eq}}$ require $N_{\text{dd}} n \times m$ matrix-vector multiplications and N_{dd} linear solves of size m .

The nonlinear least-square problem (15) can be solved using (i) steepest-descent or quasi-Newton methods, or (ii) Gauss-Newton or Levenberg-Marquandt algorithms, [45].

(i) Steepest-descent or quasi Newton methods only require the explicit calculation of the objective function \mathbf{f}^{eq} and its gradient $\nabla \mathbf{f}^{\text{eq}}$, which can be computed without explicitly forming $\widehat{\mathbf{J}}_{\mathbf{F}}^{\text{eq}}$. However, these methods do not exploit the underlying least-square structure of the optimization problem and might thus exhibit slower convergence and/or might be more prone to divergent behaviors.

(ii) The Gauss-Newton method (GNM) reads as

$$\widehat{\beta}^{(k+1)} = \widehat{\beta}^{(k)} - \left(\nabla_{\mathbf{r}^{\text{eq}}} \left(\widehat{\beta}^{(k)} \right) \right)^\dagger \mathbf{r}^{\text{eq}} \left(\widehat{\beta}^{(k)} \right)$$

where $(\cdot)^\dagger$ denotes the Moore-Penrose pseudo-inverse. The Levenberg-Marquandt algorithm (LMA) is a generalization of GNM that is typically more robust for poor choices of the initial condition. Note that GNM/LMA are the methods of choice for least-squares problems; however, they require the assembly of $\widehat{\mathbf{J}}_{\mathbf{F}}^{\text{eq}}$ at each iteration.

Algorithm 1 Solution to (15) through the Gauss-Newton method.

Inputs: $\boldsymbol{\alpha}^{(0)} = [\boldsymbol{\alpha}_1^{(0)}, \dots, \boldsymbol{\alpha}_{N_{\text{dd}}}^{(0)}]$, $\boldsymbol{\beta}^{(0)} = [\boldsymbol{\beta}_1^{(0)}, \dots, \boldsymbol{\beta}_{N_{\text{dd}}}^{(0)}]$ initial conditions (cf. Eq. (20)), $tol > 0, \text{maxit}$.

Outputs: $\widehat{\boldsymbol{\beta}}$ port coefficients, $\widehat{\boldsymbol{\alpha}} = \widehat{\mathbf{F}}^{\text{eq}}(\widehat{\boldsymbol{\beta}})$ bubble coefficients.

- 1: Compute the matrices \mathbf{P}, \mathbf{Q} in (15d).
 - 2: Set $\widehat{\boldsymbol{\beta}}^{(0)} = \boldsymbol{\beta}^{(0)}$ and $\widehat{\boldsymbol{\alpha}} = \boldsymbol{\alpha}^{(0)}$.
 - 3: **for** $k = 1, \dots, \text{maxit}$ **do**
 - 4: **for** $i = 1, \dots, N_{\text{dd}}$ **do**
 - 5: Compute $\boldsymbol{\alpha}_i$ s.t. $\widehat{\mathbf{R}}_i^{\text{eq}}(\boldsymbol{\alpha}_i, \boldsymbol{\beta}_i^{(k)}) = \mathbf{0}$ using Newton's method with initial condition $\widehat{\boldsymbol{\alpha}}_i$.
 - 6: Compute $\widehat{\mathbf{J}}_{\mathbf{F}_i}^{\text{eq}}(\boldsymbol{\beta}_i^{(k)})$ (cf. (16)).
 - 7: **end for**
 - 8: Update $\widehat{\boldsymbol{\alpha}} = [\boldsymbol{\alpha}_1, \dots, \boldsymbol{\alpha}_{N_{\text{dd}}}]$.
 - 9: Compute $\mathbf{r}^{\text{eq},(k)} = \mathbf{P}\widehat{\boldsymbol{\alpha}} + \mathbf{Q}\widehat{\boldsymbol{\beta}}^{(k)}$ and $\nabla \mathbf{r}^{\text{eq},(k)} = \mathbf{P}\widehat{\mathbf{J}}_{\mathbf{F}}^{\text{eq}} + \mathbf{Q}$.
 - 10: Compute $\widehat{\boldsymbol{\beta}}^{(k+1)} = \widehat{\boldsymbol{\beta}}^{(k)} - (\nabla \mathbf{r}^{\text{eq},(k)})^\dagger \mathbf{r}^{\text{eq},(k)}$
 - 11: **if** $\|\widehat{\boldsymbol{\beta}}^{(k+1)} - \widehat{\boldsymbol{\beta}}^{(k)}\|_2 < tol \|\widehat{\boldsymbol{\beta}}^{(k)}\|_2$ **then**, BREAK
 - 12: **end if**
 - 13: **end for**
 - 14: Return $\widehat{\boldsymbol{\beta}} = \widehat{\boldsymbol{\beta}}^{(k+1)}$ and $\widehat{\boldsymbol{\alpha}} = \widehat{\mathbf{F}}^{\text{eq}}(\widehat{\boldsymbol{\beta}})$.
-

Algorithm 1 summarizes the overall procedure as implemented in our code, which relies on GNM to solve (15); we envision that our approach can cope with LMA with only minor changes: we omit the details. Note that we update at each iteration the estimates of the bubble coefficients: this is important to speed up the solution to the local Newton problems. In addition, the algorithm requires to provide an initial guess for port and bubble coefficients; we discuss the choice of the initial condition in section 3 (cf. Eq. (20)).

As explained in [41], for nonlinear least-squares problems of the form (15d), Gauss-Newton's method shows quadratic convergence if $\mathbf{r}^{\text{eq}}(\widehat{\boldsymbol{\beta}}) = \mathbf{0}$ and a super-linear convergence if $\|\mathbf{r}^{\text{eq}}(\widehat{\boldsymbol{\beta}})\|_2$ is small. In the numerical results, we also investigate performance of a quasi-Newton method — the limited-memory BFGS method [45]. Note that the implementation of the latter follows a similar procedure as in Algorithm 1 with only minor changes: we omit the details.

Remark 2.5. *We remark that the internal loop at lines 4-7 in Algorithm 1 and the construction of the matrices \mathbf{P}, \mathbf{Q} are embarrassingly parallelizable.*

3 Methodology

3.1 Data compression

In this work, we resort to global solves to construct the archetype ROB's $\{(Z_\ell^{\text{a,b}}, W_\ell^{\text{a,b}})\}_{\ell \in \mathcal{L}}$, $Z_\ell^{\text{a,b}} = [\zeta_{\ell,1}^{\text{a,b}}, \dots, \zeta_{\ell,n}^{\text{a,b}}]$, $W_\ell^{\text{a,p}} = [\psi_{\ell,1}^{\text{a,p}}, \dots, \psi_{\ell,n}^{\text{a,p}}]$. We generate n_{train} global configurations $\{\mu^{(k)}\}_{k=1}^{n_{\text{train}}}$ and we denote by $\{(\Omega_i^{(k)}, \mathbf{L}_i^{(k)})\}_{i,k}$ the corresponding labeled partitions; we estimate the global solutions $\{u^{(k)}\}_{k=1}^{n_{\text{train}}}$ using a standard FE solver and we assemble the datasets

$$\mathcal{D}_\ell = \left\{ u^{(k)}|_{\Omega_i^{(k)}} \circ \Phi_i^{(k)} : \mathbf{L}_i^{(k)} = \ell, k = 1, \dots, n_{\text{train}} \right\} \subset \mathcal{X}_\ell^{\text{a}}, \quad \ell \in \mathcal{L}; \quad (17\text{a})$$

we further define the bubble and port datasets

$$\mathcal{D}_\ell^{\text{b}} := \{w - \mathbf{E}_\ell^{\text{a}}(w|_{\Gamma_\ell^{\text{a}}}) : w \in \mathcal{D}_\ell\}, \quad \mathcal{D}_\ell^{\text{p}} := \{\mathbf{E}_\ell^{\text{a}}(w|_{\Gamma_\ell^{\text{a}}}) : w \in \mathcal{D}_\ell\}; \quad (17\text{b})$$

finally, we apply proper orthogonal decomposition (POD, [58]) based on the method of snapshots [52] with inner product $(\cdot, \cdot)_\ell$, to obtain the local approximation spaces. Algorithm 2 summarizes the computational procedure.

In view of the application of the empirical quadrature procedures described in sections 3.2 and 3.3.1, for all $\ell \in \mathcal{L}$ we further compute the projected coefficients $\{\boldsymbol{\alpha}_{\ell,j}\}_{j=1}^{n_{\text{train},\ell}}, \{\boldsymbol{\beta}_{\ell,j}\}_{j=1}^{n_{\text{train},\ell}}$

$$(\boldsymbol{\alpha}_{\ell,j})_i = \left(u_{\ell,j}^{\text{b}}, \zeta_{\ell,i}^{\text{a,b}} \right)_\ell, \quad (\boldsymbol{\beta}_{\ell,j})_q = \left(u_{\ell,j}^{\text{p}}, \psi_{\ell,q}^{\text{a,p}} \right)_\ell, \quad \ell \in \mathcal{L}, \quad (18)$$

for $i = 1, \dots, n$, $q = 1, \dots, m$, $j = 1, \dots, n_{\text{train},\ell}$, where $u_{\ell,j}^b$ (resp., $u_{\ell,j}^p$) denotes the j -th bubble (resp., port) solution in the dataset \mathcal{D}_ℓ^b (resp., \mathcal{D}_ℓ^p).

Algorithm 2 Data compression based on global solves

Inputs: training parameters $\{\mu^{(k)}\}_{k=1}^{n_{\text{train}}}$; m, n ROB dimensions.

Outputs: $\{(Z_\ell^{\text{a,b}}, W_\ell^{\text{a,b}})\}_{\ell \in \mathcal{L}}$ ROBs; $\{\alpha_\ell^{(k)}\}_{k=1}^{n_{\text{train},\ell}}$, $\{\beta_\ell^{(k)}\}_{k=1}^{n_{\text{train},\ell}}$ local optimal coefficients.

- 1: Initialize $\mathcal{D}_\ell^b = \mathcal{D}_\ell^p = \emptyset$ for $\ell \in \mathcal{L}$.
 - 2: **for** $k = 1, \dots, n_{\text{train}}$ **do**
 - 3: Estimate the global solution u_μ to (8) using a global FE method.
 - 4: Update the datasets \mathcal{D}_ℓ^b and \mathcal{D}_ℓ^p using (17b).
 - 5: **end for**
 - 6: Perform POD to obtain the ROBs $Z_\ell^{\text{a,b}} = [\zeta_{\ell,1}^{\text{a,b}}, \dots, \zeta_{\ell,n}^{\text{a,b}}]$ and $W_\ell^{\text{a,p}} = [\psi_{\ell,1}^{\text{a,b}}, \dots, \psi_{\ell,n}^{\text{a,b}}]$
 - 7: Define the optimal coefficients $\{\alpha_\ell^{(k)}\}_{k=1}^{n_{\text{train},\ell}}$, $\{\beta_\ell^{(k)}\}_{k=1}^{n_{\text{train},\ell}}$ using (18).
-

We remark that the proposed approach — which was previously considered in [46] — might be highly inefficient since it requires global solves that are often unfeasible in the framework of CB-pMOR. We envision to further extend the localized training approach in [54] to address this issue. For practical applications, we envision that global solves should be performed using a standard FE solver and then resorting to FE interpolation routines to extract the local solutions: this procedure inevitably introduces an error at the scale of the FE mesh size between full-order and reduced-order models. Even if this error might be negligible for applications, it hinders the interpretations of the numerical investigations. To avoid this issue, in the numerical experiments, we rely on the HF model (11) to generate the dataset of local solutions.

3.2 Hyper-reduction of port-to-bubble problems

We here rely on element-wise EQ, that is we replace the residuals (5) in (13a) with the weighted residual associated with the variational form

$$\mathbb{G}_\ell^{\text{a,eq}}(w, v; \mu_\ell) = \sum_{k=1}^{N_\ell^e} \rho_{\ell,k}^{\text{eq}} \left(\int_{\mathcal{D}_{\ell,k}} \eta_\ell^{\text{a,e}}(w, v; \mu_\ell) dx + \int_{\partial \mathcal{D}_{\ell,k}} \eta_\ell^{\text{a,f}}(w, v; \mu_\ell) dx \right), \quad (19)$$

where $\rho_\ell^{\text{eq}} = [\rho_{\ell,1}^{\text{eq}}, \dots, \rho_{\ell,N_\ell^e}^{\text{eq}}]^T$ is a sparse vector of non-negative weights.

This hyper-reduction approach, which has been considered in a number of previous works including [32], is discussed for completeness in A. We anticipate that the algorithm takes as input the projected coefficients (18) generated by Algorithm 2 and the associated local parameters, $\{(\alpha_\ell^{(j)}, \beta_\ell^{(j)}, \mu_\ell^{(j)})\}_{j=1}^{n_{\text{train},\ell}}$.

We remark that, as discussed in [20], the use of elementwise- (as opposed to pointwise-) reduced quadrature formulations leads to significantly less efficient ROMs, particularly for high-order FE discretizations. On the other hand, elementwise reduced quadrature formulations are significantly easier to implement and can easily cope with geometry deformations [57]. We refer to [23, 61, 62] for a thorough introduction to state-of-the-art hyper-reduction techniques.

3.3 Hyper-reduction of the objective function

Exploiting (15b), it is easy to verify that — we here stress dependence on the parameter value μ —

$$\mathfrak{F}(\alpha, \beta, \{\rho_\ell^{\text{p,eq}}\}_{\ell \in \mathcal{L}}, \mu) = \frac{1}{2} \sum_{\ell \in \mathcal{L}} \left(\sum_{i: \text{Li}=\ell} \eta_i^{\text{p}}(\alpha, \beta, \mu) \right) \cdot \rho_\ell^{\text{p,eq}} = \frac{1}{2} \sum_{\ell \in \mathcal{L}} \sum_{j=1}^{N_{\text{dd},\ell}} (\mathbf{G}_\ell^{\text{p}}(\alpha, \beta, \mu) \rho_\ell^{\text{p,eq}})_j,$$

where $N_{\text{dd},\ell}$ is the number of components of type ℓ and $\{\mathbf{G}_\ell^{\text{p}}\}_\ell$ are suitable matrices; to provide a concrete example, for the model problem of section 2.2, we have

$$\mathbf{G}_{\text{int}}^{\text{p}}(\alpha, \beta, \mu) = \begin{bmatrix} (\eta_1^{\text{p}}(\alpha, \beta, \mu))^T \\ \vdots \\ (\eta_{Q_a}^{\text{p}}(\alpha, \beta, \mu))^T \end{bmatrix}, \quad \mathbf{G}_{\text{ext}}^{\text{p}}(\alpha, \beta, \mu) = (\eta_{Q_a+1}^{\text{p}}(\alpha, \beta, \mu))^T.$$

In order to speed up the evaluation of \mathbf{f}^{eq} , it is necessary to build a sparse quadrature rule $\{\boldsymbol{\rho}_\ell^{\text{p,eq}}\}_{\ell \in \mathcal{L}}$. In the remainder of this section, we propose two different strategies to address this task: the former relies on the solution to a suitable sparse representation problem and is tightly linked to the EQ procedure employed for hyper-reduction of the port-to-bubble maps; the latter relies on a variant of the empirical interpolation method (EIM, [4]) for vector-valued functions.

3.3.1 Empirical quadrature method

We denote by $(\boldsymbol{\alpha}^{(k)}, \boldsymbol{\beta}^{(k)})$ the projected bubble and port coefficients associated with the k -th configuration $\mu^{(k)}$ and Eq. (18); we further denote by $(\boldsymbol{\alpha}_0^{(k)}, \boldsymbol{\beta}_0^{(k)})$ the bubble and port coefficients associated with the sample means,

$$\boldsymbol{\alpha}_0^{(k)} = \begin{bmatrix} \boldsymbol{\alpha}_{0,1}^{(k)} \\ \vdots \\ \boldsymbol{\alpha}_{0,N_{\text{dd}}^{(k)}}^{(k)} \end{bmatrix}, \quad \boldsymbol{\beta}_0^{(k)} = \begin{bmatrix} \boldsymbol{\beta}_{0,1}^{(k)} \\ \vdots \\ \boldsymbol{\beta}_{0,N_{\text{dd}}^{(k)}}^{(k)} \end{bmatrix}, \quad k = 1, \dots, n_{\text{train}}, \quad (20a)$$

where $\boldsymbol{\alpha}_{0,i}^{(k)} = \boldsymbol{\alpha}_{L_i^{(k)}}^{\text{avg}}$ and $\boldsymbol{\beta}_{0,i}^{(k)} = \boldsymbol{\beta}_{L_i^{(k)}}^{\text{avg}}$, with

$$\boldsymbol{\alpha}_\ell^{\text{avg}} := \frac{1}{n_{\text{train},\ell}} \sum_{j=1}^{n_{\text{train},\ell}} \boldsymbol{\alpha}_{\ell,j}, \quad \boldsymbol{\beta}_\ell^{\text{avg}} := \frac{1}{n_{\text{train},\ell}} \sum_{j=1}^{n_{\text{train},\ell}} \boldsymbol{\beta}_{\ell,j}, \quad \forall \ell \in \mathcal{L}. \quad (20b)$$

We anticipate that (20) is used in the numerical results to initialize the Gauss-Newton's algorithm.

Given the random samples $s^{(k)} \stackrel{\text{iid}}{\sim} \text{Uniform}(0, 1)$, we define the matrices

$$\mathbf{C}_\ell = \begin{bmatrix} \mathbf{G}_\ell^{\text{p}}(\tilde{\boldsymbol{\alpha}}^{(1)}, \tilde{\boldsymbol{\beta}}^{(1)}, \mu^{(1)}) \\ \vdots \\ \mathbf{G}_\ell^{\text{p}}(\tilde{\boldsymbol{\alpha}}^{(n_{\text{train}})}, \tilde{\boldsymbol{\beta}}^{(n_{\text{train}})}, \mu^{(n_{\text{train}})}) \\ \mathbf{1}^T \end{bmatrix}, \quad \forall \ell \in \mathcal{L}, \quad (21a)$$

where $\mathbf{1}$ is the vector with entries all equal to one, and $\tilde{\boldsymbol{\alpha}}^{(k)}$ and $\tilde{\boldsymbol{\beta}}^{(k)}$ are random convex interpolations between the projected bubble and port coefficients $(\boldsymbol{\alpha}^{(k)}, \boldsymbol{\beta}^{(k)})$ and the initial conditions for the GNM $(\boldsymbol{\alpha}_0^{(k)}, \boldsymbol{\beta}_0^{(k)})$,

$$\tilde{\boldsymbol{\alpha}}^{(k)} = (1 - s^{(k)})\boldsymbol{\alpha}^{(k)} + s^{(k)}\boldsymbol{\alpha}_0^{(k)}, \quad \tilde{\boldsymbol{\beta}}^{(k)} = (1 - s^{(k)})\boldsymbol{\beta}^{(k)} + s^{(k)}\boldsymbol{\beta}_0^{(k)}, \quad k = 1, \dots, n_{\text{train}}. \quad (21b)$$

The first n_{train} blocks of \mathbf{C}_ℓ are associated to the ‘‘manifold accuracy constraints’’, while the last row is associated to the ‘‘constant accuracy constraint’’ [63]. Then, we compute the empirical weights $\{\boldsymbol{\rho}_\ell^{\text{p,eq}}\}_{\ell \in \mathcal{L}}$ by approximately solving the non-negative least-square problem

$$\min_{\boldsymbol{\rho} \in \mathbb{R}^{N_\ell^{\text{p}}}} \|\mathbf{C}_\ell(\boldsymbol{\rho} - \boldsymbol{\rho}_\ell^{\text{p}})\|_2, \quad \text{s.t. } \boldsymbol{\rho} \geq 0 \quad (21c)$$

up to a tolerance $\text{tol}_{\text{eq}}^{\text{obj}}$ using the Matlab function `lsqnonneg`, which implements the iterative procedure proposed in [35].

The choice of the port and bubble coefficients $\{(\tilde{\boldsymbol{\alpha}}^{(k)}, \tilde{\boldsymbol{\beta}}^{(k)})\}_k$ for the ‘‘accuracy constraints’’ in (21a) is justified by the fact that the objective function should be accurate for all port and bubble coefficients considered during the GNM iterations; this choice is found to empirically improve the conditioning of the non-negative least-square problem and ultimately improve performance — compared to the choice $\tilde{\boldsymbol{\alpha}}^{(k)} = \boldsymbol{\alpha}^{(k)}$, $\tilde{\boldsymbol{\beta}}^{(k)} = \boldsymbol{\beta}^{(k)}$. The constant function accuracy constraint, which was first proposed in [63] for hyper-reduction of monolithic ROMs, is important to bound the ℓ^1 norm of the empirical weights; we have indeed

$$\|\boldsymbol{\rho}_\ell^{\text{p,eq}}\|_1 \leq |\mathbf{1} \cdot (\boldsymbol{\rho}_\ell^{\text{p,eq}} - \boldsymbol{\rho}_\ell^{\text{p}})| + \|\boldsymbol{\rho}_\ell^{\text{p}}\|_1 \leq \|\mathbf{C}_\ell(\boldsymbol{\rho}_\ell^{\text{p,eq}} - \boldsymbol{\rho}_\ell^{\text{p}})\|_2 + \|\boldsymbol{\rho}_\ell^{\text{p}}\|_1, \quad \forall \ell \in \mathcal{L}. \quad (22)$$

We also observe that, even if hyper-reduction is ultimately performed at the local level, for each archetype component, the EQ procedure requires global solves to define the matrices $\{\mathbf{C}_\ell\}_\ell$.

3.3.2 Empirical interpolation method

The objective function \mathfrak{F} is designed to penalize the jump of the solution at the components' interface. Since the jumps are dictated by the behavior of the port modes $\{\psi_{\ell,i}^{\text{a,p}}\}_{i=1}^m$ on the ports Γ_ℓ , we propose to replace the integral in (14) with the discrete sum

$$\frac{1}{2} \sum_{i=1}^{N_{\text{dd}}} \sum_{j \in \text{Neigh}_i} \int_{\Gamma_{i,j}} \|\widehat{u}_i(\boldsymbol{\alpha}_i, \boldsymbol{\beta}_i) - \widehat{u}_j(\boldsymbol{\alpha}_j, \boldsymbol{\beta}_j)\|_2^2 dx \approx \frac{1}{2} \sum_{q \in \mathbb{I}_\ell^{\text{p,eq}}} (\boldsymbol{\eta}_i^{\text{p}}(\boldsymbol{\alpha}, \boldsymbol{\beta}, \mu))_q, \quad (23)$$

where $\mathbb{I}_\ell^{\text{p,eq}} \subset \{1, \dots, N_\ell^{\text{p}}\}$ are chosen so that we can adequately recover any element of $\mathcal{Z}_\ell^{\text{a,p}}$ based on the information at the points $\{x_{\ell,j}^{\text{p}}\}_{j \in \mathbb{I}_\ell^{\text{p,eq}}}$. Note that the approximation (23) is an inconsistent approximation of the L^2 integral (14); however, we expect — and we verify numerically — that the minimization of the right-hand side of (23) should control the jump at elements' interfaces and ultimately ensure accurate performance.

We here rely on a variant of EIM to select the quadrature indices $\mathbb{I}_\ell^{\text{p,eq}}$. EIM was first proposed in [4] to identify accurate interpolation points for arbitrary sets of scalar functions. In this work, we resort to the extension of EIM to vector-valued fields considered in [56]. We refer to the MOR literature for other variants of EIM for vector-valued fields; in particular, we observe that the present algorithm returns exactly m quadrature points: we refer to [40, Algorithm 2] and to [14] for extensions of EIM that resort to over-collocation to improve performance.

Algorithm 3 reviews the computational procedure: note that, for each $\ell \in \mathcal{L}$, the algorithm takes as input the port functions $\{\psi_{\ell,i}^{\text{a,p}}\}_{i=1}^m$ and returns the indices $\mathbb{I}_\ell^{\text{p,eq}}$. Given the set of indices $\mathbb{I}_\ell^{\text{p,eq}}$ and the space $\mathcal{Z}_\ell^{\text{a,p}}$, we denote by $\mathcal{G}_{\ell,m}$ the approximation least-square operator

$$\mathcal{G}_{\ell,m}(v) := \mathcal{G}(v; \mathbb{I}_\ell^{\text{p,eq}}, \mathcal{Z}_\ell^{\text{a,p}}) = \arg \min_{\psi \in \mathcal{Z}_\ell^{\text{a,p}}} \sum_{j \in \mathbb{I}_\ell^{\text{p,eq}}} \|v(x_{\ell,j}^{\text{p}}) - \psi(x_{\ell,j}^{\text{p}})\|_2^2, \quad \forall v \in C(\Gamma_\ell; \mathbb{R}^D), \ell \in \mathcal{L}.$$

Note that for $D > 1$ $\mathcal{G}_{\ell,m}$ is not an interpolation operator.

Algorithm 3 Empirical Interpolation Method for vector-valued fields

Input: $\{\psi_{\ell,i}^{\text{a,p}}\}_{i=1}^m$, $\ell \in \mathcal{L}$

Output: $\mathbb{I}_\ell^{\text{p,eq}} = \{\mathbf{i}_{\ell,1}^*, \dots, \mathbf{i}_{\ell,m}^*\}$

Set $\mathbf{i}_{\ell,1}^* := \arg \max_{j \in \{1, \dots, N_\ell^{\text{p}}\}} \|\psi_{\ell,1}^{\text{a,p}}(x_{\ell,j}^{\text{p}})\|_2$, and define $\mathcal{G}_{\ell,1} := \mathcal{G}(\cdot; \{\mathbf{i}_{\ell,1}^*\}, \text{span}\{\psi_{\ell,1}^{\text{a,p}}\})$

for $m' = 2, \dots, m$ **do**

 Compute $r_{m'} = \psi_{\ell,m'}^{\text{a,p}} - \mathcal{G}_{\ell,m'-1}(\psi_{\ell,m'}^{\text{a,p}})$

 Set $\mathbf{i}_{\ell,m'}^* := \arg \max_{j \in \{1, \dots, N_\ell^{\text{p}}\}} \|r_{m'}(x_{\ell,j}^{\text{p}})\|_2$

 Update $\mathcal{G}_{\ell,m'} := \mathcal{G}(\cdot; \{\mathbf{i}_{\ell,j}^*\}_{j=1}^{m'}, \text{span}\{\psi_{\ell,j}^{\text{a,p}}\}_{j=1}^{m'})$.

end for

4 Analysis and interpretation for linear coercive problems

We analyze the OS2 statement for linear coercive problems. To simplify the presentation, we consider the case with two subdomains depicted in Figure 1. We denote by $(\mathcal{X}, \|\cdot\|_\Omega)$ the global ambient space such that $H_0^1(\Omega) \subset \mathcal{X} \subset H^1(\Omega)$; given the ports Γ_1, Γ_2 (cf. Figure 1), we define the bubble and port spaces:

$$\mathcal{X}_{i,0} := \{v \in \mathcal{X}_i : v|_{\Gamma_i} = 0\}, \quad \mathcal{U}_i := \{v|_{\Gamma_i} : v \in \mathcal{X}_i\}, \quad i = 1, 2.$$

We introduce the bilinear form $a : \mathcal{X} \times \mathcal{X} \rightarrow \mathbb{R}$ with continuity constant γ and coercivity constant $\alpha > 0$, and we introduce the linear functional $f \in \mathcal{X}'$. Then, we introduce the model problem:

$$\text{find } u^* \in \mathcal{X} : a(u^*, v) = f(v) \quad \forall v \in \mathcal{X}. \quad (24)$$

In section 4.1, we derive the port formulation of the problem (24); in section 4.2, we present two important results for the port problem; in section 4.3 we exploit the results of the previous section to derive an *a priori* bound for the OS2 statement; in section 4.4, we comment on an alternative variational interpretation of the OS2 statement; finally, in section 4.5, we derive explicit estimates for two representative model problems.

Given $v \in \mathcal{X}_{i,0}$, we denote by $v^{\text{ext}} \in \mathcal{X}$ the trivial extension of v to Ω that is zero in $\Omega \setminus \Omega_i$. We assume that a and f are associated to a differential (elliptic) problem; in particular, we assume that

$$a(u, v^{\text{ext}}) = a(u|_{\Omega_i}, v), \quad \forall v \in \mathcal{X}_{i,0}. \quad (25)$$

Note that by construction we have $f(v^{\text{ext}}) = f(v)$ for all $v \in \mathcal{X}_{i,0}$.

4.1 Port formulation

We define the tensor-product space $\mathcal{U} = \mathcal{U}_1 \times \mathcal{U}_2$ endowed with the inner product $\langle w, v \rangle = \sum_{i=1,2} (w_i, v_i)_{H^{1/2}(\Gamma_i)}$ and the induced norm $\| \cdot \| = \sqrt{\langle \cdot, \cdot \rangle}$. We introduce the local solution operators $T_i : \mathcal{U}_i \rightarrow \mathcal{X}_i$ and $G_i : \mathcal{X}' \rightarrow \mathcal{X}_{i,0}$ such that:

$$(T_i \lambda)|_{\Gamma_i} = \lambda, \quad a(T_i \lambda, v) = 0 \quad \forall v \in \mathcal{X}_{i,0}; \quad (26)$$

$$(G_i f)|_{\Gamma_i} = 0, \quad a(G_i f, v) = f(v) \quad \forall v \in \mathcal{X}_{i,0}. \quad (27)$$

Since the elements of $\mathcal{X}_{i,0}$ can be trivially extended to zero in $\Omega \setminus \Omega_i$, we have that the form a is continuous and coercive in $\mathcal{X}_{i,0}$ with continuity and coercivity constants bounded from above and below by γ and α , due to the fact that $\mathcal{X}_{i,0} \subset \mathcal{X}$.

Therefore, T_i and G_i are well-defined linear bounded operators. By comparing the previous definitions with (11a), we note that the affine operators $F_i := T_i - E_i + G_i f$ correspond to the port-to-bubble maps that are exploited to derive the hybridized formulation in section 2: we have $u^*|_{\Omega_i} = F_i \lambda_i^* + E_i \lambda_i^* = T_i \lambda_i^* + G_i f$, where $\lambda_i^* \in \mathcal{U}_i$ is equal to $u^*|_{\Gamma_i}$.

Given the trace operators $\chi_{\Gamma_1} : \mathcal{X}_2 \rightarrow \mathcal{U}_1$, $\chi_{\Gamma_2} : \mathcal{X}_1 \rightarrow \mathcal{U}_2$, we introduce the operators $T : \mathcal{U} \rightarrow \mathcal{U}$ and $G : \mathcal{X}' \rightarrow \mathcal{U}$ such that

$$T\lambda = \begin{bmatrix} \chi_{\Gamma_1} T_2 \lambda_2 \\ \chi_{\Gamma_2} T_1 \lambda_1 \end{bmatrix}, \quad Gf = \begin{bmatrix} \chi_{\Gamma_1} G_2 f \\ \chi_{\Gamma_2} G_1 f \end{bmatrix}, \quad \forall \lambda \in \mathcal{U}, \quad f \in \mathcal{X}'. \quad (28a)$$

Finally, we introduce the port problem: find $\lambda^* \in \mathcal{U}$ such that

$$a_p(\lambda^*, v) = f_p(v) \quad \forall v \in \mathcal{U}, \quad \text{where } a_p(\lambda, v) := \langle \lambda - T\lambda, v \rangle, \quad f_p(v) := \langle Gf, v \rangle. \quad (28b)$$

Remark 4.1. Connection with OS methods. We can rewrite standard additive and multiplicative OS iterations using the operators introduced in (28). In more detail, multiplicative OS iterations can be written as (see, e.g., [48, Chapter 1])

$$\begin{bmatrix} Id & 0 \\ -\chi_{\Gamma_2} T_1 & Id \end{bmatrix} \lambda^{(k+1)} = \begin{bmatrix} 0 & \chi_{\Gamma_1} T_2 \\ 0 & 0 \end{bmatrix} \lambda^{(k)} + Gf, \quad k = 1, 2, \dots,$$

while additive OS iterations can be written as

$$\begin{bmatrix} Id & 0 \\ 0 & Id \end{bmatrix} \lambda^{(k+1)} = \begin{bmatrix} 0 & \chi_{\Gamma_1} T_2 \\ \chi_{\Gamma_2} T_1 & 0 \end{bmatrix} \lambda^{(k)} + Gf, \quad k = 1, 2, \dots$$

These identities imply that any fixed point of the OS iterations satisfies (28b) and thus OS and OS2 converge to the same limit as $k \rightarrow +\infty$. As discussed in the introduction, this connection between OS and OS2 formulations is valid for both linear and nonlinear problems; however, the analysis is strictly restricted to the linear case.

4.2 Analysis of the port problem

Theorem 4.1 clarifies the relationship between the variational statement (24) and the port problem (28); on the other hand, Theorem 4.2 is key for the analysis of the OS2 ROM. Proofs are postponed to B. The results rely on the introduction of a partition-of-unity (PoU, [1]) $\{\phi_i\}_{i=1}^2 \subset \text{Lip}(\Omega; \mathbb{R})$ associated with $\{\Omega_i\}_{i=1}^2$ such that

$$\sum_{i=1}^2 \phi_i(x) = 1, \quad \begin{cases} 0 \leq \phi_i(x) \leq 1 & \forall x \in \Omega, \\ \phi_i(x) = 0 & \forall x \notin \Omega_i, \end{cases} \quad i = 1, 2.$$

Proposition 4.1. Let u^* be the solution to (24). Then, $\lambda^* = (u^*|_{\Gamma_1}, u^*|_{\Gamma_2})$ solves (28b). Conversely, if λ^* is a solution to (28b), then $u^* = \sum_{i=1}^2 (T_i \lambda_i^* + G_i f) \phi_i$ solves (24).

Proposition 4.2. Let the operator T in (28a) be compact. Then, the form $a_p : \mathcal{U} \times \mathcal{U} \rightarrow \mathbb{R}$ defined in (28b) is inf-sup stable and continuous, that is

$$\alpha_p = \inf_{w \in \mathcal{U}} \sup_{v \in \mathcal{U}} \frac{a_p(w, v)}{\|w\| \|v\|} > 0, \quad \gamma_p = \sup_{w \in \mathcal{U}} \sup_{v \in \mathcal{U}} \frac{a_p(w, v)}{\|w\| \|v\|} < \infty. \quad (29)$$

The proof of the compactness of the operator T depends on the underlying PDE. For several problems, including the Laplace equation, the advection-diffusion-reaction equation, the Stokes equations, and the Helmholtz's equation, we can prove compactness of the operator T using Caccioppoli's inequalities: we refer to [55, Appendix C] and also [53] for further details. We further observe that Theorem 4.2 does not provide an explicit relationship among the stability constant α_p in Theorem 4.2, the PDE of interest and the size of the overlap. We envision that the derivation of explicit bounds for the stability constant α_p in terms of the PDE of interest and the size of the overlap will shed light on the underlying properties of the OS2 formulation and might also lead to new algorithmic developments. We note that there is a vast body of works that address the derivation of sharp estimates for the convergence of overlapping Schwarz methods (see, e.g., [11, 15]): the derivation of analogous results for this setting is beyond the scope of the present paper.

As discussed in B, proofs of Propositions 4.1 and 4.2 rely on the fact that, if we introduce the spaces $\mathcal{X}_{1,2} = \{v|_{\Omega_1 \cap \Omega_2} : v \in \mathcal{X}\}$ and $\mathcal{X}_{1,2}^0 = \{v \in \mathcal{X}_{1,2} : v|_{\Gamma_1 \cup \Gamma_2} = 0\}$, the problem of finding $u \in \mathcal{X}_{1,2}$ such that

$$a(u, v) = 0 \quad \forall v \in \mathcal{X}_{1,2}^0, \quad u|_{\Gamma_1} = \lambda_1, \quad u|_{\Gamma_2} = \lambda_2,$$

admits a unique solution for any $(\lambda_1, \lambda_2) \in \mathcal{U}$. This result is trivial for coercive problems, but it is significantly less trivial — and requires additional assumptions — for inf-sup stable problems and is not addressed in this work. On the other hand, we envision that the analysis for nonlinear PDEs requires more sophisticated tools and is beyond the scope of this work.

4.3 Analysis of the OS2 statement

We consider the following OS2 formulation for the linear problem (24):

$$\text{find } \hat{\lambda} = \arg \min_{\lambda \in \mathcal{Z}^p} \left\| \lambda - \hat{T}\lambda - \hat{G}f \right\|. \quad (30)$$

Note that (30) corresponds to the OS2 statement (11) with the important difference that we replace the L^2 norm with the $H^{1/2}$ norm $\|\cdot\|$. In particular, in our work, the space \mathcal{Z}^p in (30) is given by the tensor product of the local port spaces, $\mathcal{Z}^p = \mathcal{Z}_1^p \times \mathcal{Z}_2^p$, and \hat{T}, \hat{G} are associated to the approximate local solution operators that are obtained by Galerkin projection. We further introduce the OS2 formulation with perfect local operators:

$$\text{find } \tilde{\lambda} = \arg \min_{\lambda \in \mathcal{Z}^p} \|\lambda - T\lambda - Gf\|. \quad (31)$$

We observe that (31) corresponds to the minimum residual formulation of the port problem (28); we have indeed

$$\|\lambda - T\lambda - Gf\| = \sup_{v \in \mathcal{U}} \frac{\langle \lambda - T\lambda - Gf, v \rangle}{\|v\|} = \sup_{v \in \mathcal{U}} \frac{a_p(\lambda, v) - f_p(v)}{\|v\|}.$$

Recalling the result in [60], we thus have

$$\left\| \lambda^* - \tilde{\lambda} \right\| \leq \frac{\gamma_p}{\alpha_p} \inf_{\lambda \in \mathcal{Z}^p} \|\lambda^* - \lambda\|, \quad (32)$$

which proves the quasi-optimality of the OS2 statement with perfect local operators (31).

To estimate the error $\left\| \hat{\lambda} - \tilde{\lambda} \right\|$, we resort to a perturbation analysis. We denote by $\hat{\alpha}_p$ and $\hat{\gamma}_p$ the stability and continuity constants associated with the problem (30): it is possible to resort to a perturbation analysis to estimate these constants; since the argument is completely standard, we omit the details. We define the quantities ε_T and ε_G as follows:

$$\varepsilon_T := \sup_{\psi \in \mathcal{Z}^p} \frac{\left\| (T - \hat{T})\psi \right\|}{\|\psi\|}, \quad \varepsilon_G := \left\| (G - \hat{G})f \right\|. \quad (33)$$

Then, it is possible to show that

$$\left\| \tilde{\lambda} - \hat{\lambda} \right\| \leq \frac{1}{\alpha_p^2} \left(M(\gamma_p + \hat{\gamma}_p) \frac{\left\| \hat{G}f \right\|}{\hat{\alpha}_p} \varepsilon_T + \sqrt{M} \left(\hat{\gamma}_p \varepsilon_G + \left\| \hat{G}f \right\| \varepsilon_T \right) \right). \quad (34)$$

We postpone the proof of (34) to B.

By combining (34) with (32), we obtain the following result. We observe that (35) is the sum of two terms: the first term is associated with the approximation properties of the port space, while the second term is directly linked to the accuracy of the local solution operators.

Proposition 4.3. Let γ_p, α_p be the continuity and stability constants of the form a_p and let $\widehat{\gamma}_p, \widehat{\alpha}_p$ be the continuity and stability constants of the form $\widehat{a}_p(\lambda, v) = \langle \lambda - \widehat{T}\lambda, v \rangle$. Given the M -dimensional space $\mathcal{Z}^p \subset \mathcal{U}$, we have

$$\left\| \lambda^* - \widehat{\lambda} \right\| \leq \frac{1}{\alpha_p} \left(\gamma_p \inf_{\lambda \in \mathcal{Z}^p} \|\lambda^* - \lambda\| + \frac{1}{\alpha_p} \left(M(\gamma_p + \widehat{\gamma}_p) \frac{\|\widehat{G}f\|}{\widehat{\alpha}_p} \varepsilon_T + \sqrt{M} \left(\widehat{\gamma}_p \varepsilon_G + \|\widehat{G}f\| \varepsilon_T \right) \right) \right). \quad (35)$$

4.4 Alternative variational interpretation of the OS2 statement

Following [38], we might also consider the alternative variational framework of the OS limit formulation (see also [48, Chapter 1.5.2]): find $(u_1^b, u_1^p, u_2^b, u_2^p) \in \bigotimes_{i=1}^2 \mathcal{X}_{i,0} \times \mathcal{U}_i$ such that

$$\begin{cases} a(u_i^b + E_i u_i^p, v_i) = f(v_i) & \forall v_i \in \mathcal{X}_{i,0}, \quad i = 1, 2; \\ (u_1^p - \chi_{\Gamma_1}(u_2^b + E_2 u_2^p), \psi_1)_{H^{1/2}(\Gamma_1)} + (u_2^p - \chi_{\Gamma_2}(u_1^b + E_1 u_1^p), \psi_2)_{H^{1/2}(\Gamma_2)} = 0 & \forall \psi = (\psi_1, \psi_2) \in \mathcal{U}; \end{cases} \quad (36)$$

where E_1, E_2 are the extension operators, u_1^b, u_2^b are the bubble solutions and u_1^p, u_2^p are the port solutions. Given the reduced spaces $\mathcal{Z}_i^b \subset \mathcal{X}_{i,0}$ and $\mathcal{Z}_i^p \subset \mathcal{U}_i$, and the approximate port-to-bubble maps $\widehat{F}_i = \widehat{T}_i + \widehat{G}_i f - E_i$, for $i = 1, 2$, the reduced-order OS2 formulation can be stated as follows: find $(\widehat{u}_1^b, \widehat{u}_1^p, \widehat{u}_2^b, \widehat{u}_2^p) \in \bigotimes_{i=1}^2 \mathcal{Z}_i^b \times \mathcal{Z}_i^p$ such that

$$\begin{cases} a(\widehat{u}_i^b + E_i \widehat{u}_i^p, v_i) = f(v_i) & \forall v_i \in \mathcal{Z}_i^b, \quad i = 1, 2; \\ (\widehat{u}_1^p - \chi_{\Gamma_1}(\widehat{u}_2^b + E_2 \widehat{u}_2^p), \psi_1)_{H^{1/2}(\Gamma_1)} + (\widehat{u}_2^p - \chi_{\Gamma_2}(\widehat{u}_1^b + E_1 \widehat{u}_1^p), \psi_2)_{H^{1/2}(\Gamma_2)} = 0 & \forall \psi = (\psi_1, \psi_2) \in \widetilde{\mathcal{Z}}^p; \end{cases} \quad (37a)$$

where $\widetilde{\mathcal{Z}}^p \subset \mathcal{U}$ is the M -dimensional space given by

$$\widetilde{\mathcal{Z}}^p = \left\{ \left(\zeta_1^p - \chi_{\Gamma_1} \widehat{T}_2(\zeta_2^p), \zeta_2^p - \chi_{\Gamma_2} \widehat{T}_1(\zeta_1^p) \right) : \zeta_i^p \in \mathcal{Z}_i^p, i = 1, 2 \right\}, \quad (37b)$$

and $\widehat{T}_i \zeta$ satisfies $\widehat{T}_i \zeta = u^b(\zeta) + E_i \zeta$ with $u_i^b(\zeta) \in \mathcal{Z}_i^b$ and $a(u_i^b(\zeta) + E_i \zeta, v) = 0$ for all $v \in \mathcal{Z}_i^b$.

The proof of (37) is straightforward, and it is provided for completeness in B. Note that the OS2 statement reads as a Petrov-Galerkin projection of (36) for a suitable choice of the test space $\widetilde{\mathcal{Z}}^p$. We envision that (37) could be exploited to devise an alternative error analysis for the OS2 statement. We do not address this issue in the present work.

4.5 Explicit convergence rates for two one-dimensional model problems

Given $\Omega = (-1, 1)$ and the partition $\Omega_1 = (-1, \delta)$, $\Omega_2 = (-\delta, 1)$, we study the convergence of (multiplicative) OS and OS2 for the problems

$$\begin{cases} u'' = 2 & \text{in } \Omega, \\ u(-1) = u(1) = 1; \end{cases} \quad (38a)$$

and

$$\begin{cases} -u'' + \gamma u' = 0 & \text{in } \Omega, \\ u(-1) = 0, \quad u(1) = 1; \end{cases} \quad (38b)$$

in the limit $|\delta| \ll 1$.

The analysis can be readily extended to the additive OS method.

For OS2, we resort to the gradient descent method with optimal choice of the step size, and to the Gauss-Newton method (OS2-GN) — the choice of the gradient descent method is intended to simplify calculations (compared to quasi-Newton methods). The motivation of this analysis is twofold: first, we show that the use of gradient-based methods — as opposed to Gauss-Newton — is increasingly sub-optimal as $\delta \rightarrow 0$; second, we provide explicit estimates for the constants α_p and γ_p of Proposition 4.2 for two representative model problems.

We denote by \widehat{u}_i the approximation of the solution in Ω_i for $i = 1, 2$; we define $\beta_1 = \widehat{u}_1(\delta)$ and $\beta_2 = \widehat{u}_2(-\delta)$. We can show that OS and OS2 iterations can be written as

$$\beta^{(k)} = \mathbf{P}_\delta^{\text{os}} \beta^{(k-1)} + \mathbf{F}_\delta^{\text{os}}, \quad \beta^{(k)} = \mathbf{P}_\delta^{\text{os2}} \beta^{(k-1)} + \mathbf{F}_\delta^{\text{os2}},$$

for $k = 1, 2, \dots$ and suitable choices of $(\mathbf{P}_\delta^{\text{os}}, \mathbf{F}_\delta^{\text{os}})$ and $(\mathbf{P}_\delta^{\text{os2}}, \mathbf{F}_\delta^{\text{os2}})$. On the other hand, since the problems are linear, OS2-GN reduces to a direct method and can be stated as

$$\mathbf{A}_\delta \beta = \mathbf{F}_\delta$$

for suitable choices of $(\mathbf{A}_\delta, \mathbf{F}_\delta)$.

In B, we show that the spectral radii ρ_δ^{os} and $\rho_\delta^{\text{os}2}$ of the transition matrices $\mathbf{P}_\delta^{\text{os}}$ and $\mathbf{P}_\delta^{\text{os}2}$ satisfy

$$\begin{aligned} \rho_\delta^{\text{os}} &\sim 1 - 4\delta, & \rho_\delta^{\text{os}2} &\sim 1 - 4\delta^2 & \text{for (38a);} \\ \rho_\delta^{\text{os}} &\sim 1 - 2\frac{e^\gamma + 1}{e^\gamma - 1}\gamma\delta, & \rho_\delta^{\text{os}2} &\sim 1 - \frac{e^\gamma + 2}{8(e^\gamma - 1)}\gamma^2\delta^2 & \text{for (38b);} \end{aligned} \quad (39a)$$

while the condition number of the linear system associated to OS2-GN satisfies

$$\begin{aligned} \text{cond}(\mathbf{A}_\delta) &= \frac{1}{\delta}, & \text{for (38a);} \\ \text{cond}(\mathbf{A}_\delta) &\sim \frac{4(e^\gamma - 1)}{4(e^\gamma + 2)\gamma}\delta^{-1} & \text{for (38b);} \end{aligned} \quad (39b)$$

and the constants α_p and γ_p defined in Theorem 4.2 satisfy

$$\begin{aligned} \alpha_p &= \frac{2\delta}{1 + \delta}, \quad \gamma_p = \frac{2}{1 + \delta}, & \text{for (38a);} \\ \alpha_p &\sim \frac{4(e^\gamma + 2)\gamma\delta}{2(e^\gamma - 1)}, \quad \gamma_p \sim 2, & \text{for (38b);} \end{aligned} \quad (39c)$$

As expected, OS, OS2 and OS2-GN become increasingly ill-conditioned as δ decreases to zero and do not converge for $\delta = 0$; however, we observe that for small values of δ OS exhibits significantly faster convergence rates than OS2 based on the gradient-descent method: this observation further strengthens the importance of exploiting the least-square structure of the OS2 statement.

5 Numerical results

5.1 Assessment metrics and training parameters

We train the CB-ROM based on $n_{\text{train}} = 70$ global parameters $\Xi_{\text{train}} = \{\mu^{(k)}\}_{k=1}^{n_{\text{train}}}$ such that

$$(E_1^{(k)}, E_2^{(k)}, E_3^{(k)}, s^{(k)}) \stackrel{\text{iid}}{\sim} \text{Uniform}([25, 30] \times [10, 20]^2 \times [0.4, 1]), \quad Q_a^{(k)} \stackrel{\text{iid}}{\sim} \text{Uniform}(\{2, \dots, 7\});$$

on the other hand, we assess performance based on $n_{\text{test}} = 20$ out-of-sample global parameters $\Xi_{\text{test}} = \{\tilde{\mu}^{(j)}\}_{j=1}^{n_{\text{test}}}$ generated using the same distribution. In view of the assessment, we also define the PoU $\{\phi_i\}_{i=1}^{N_{\text{dd}}} \subset \text{Lip}(\Omega; \mathbb{R})$ associated with the partition $\{\Omega_i\}_{i=1}^{N_{\text{dd}}}$ such that

$$\sum_{i=1}^{N_{\text{dd}}} \phi_i(x) = 1, \quad \begin{cases} 0 \leq \phi_i(x) \leq 1 & \forall x \in \Omega, \\ \phi_i(x) = 0 & \forall x \notin \Omega_i, \end{cases} \quad i = 1, \dots, N_{\text{dd}}.$$

Given $u \in \mathcal{X} := \bigotimes_{i=1}^{N_{\text{dd}}} \mathcal{X}_i$, we define the PoU operator

$$\mathbb{P}_{\text{pu}}[u] := \sum_{i=1}^{N_{\text{dd}}} \phi_i u_i \in H^1(\Omega). \quad (40)$$

Note that we omit the dependence of $\{\phi_i\}_i$ and also N_{dd} on the parameter to shorten notation. Finally, we define the out-of-sample average and maximum prediction errors

$$E_{\text{avg}} := \frac{1}{n_{\text{test}}} \sum_{\mu \in \Xi_{\text{test}}} \frac{\|\mathbb{P}_{\text{pu}}[u_\mu^{\text{hf}}] - \mathbb{P}_{\text{pu}}[\widehat{u}_\mu]\|_{H^1(\Omega)}}{\|\mathbb{P}_{\text{pu}}[u_\mu^{\text{hf}}]\|_{H^1(\Omega)}}, \quad (41a)$$

$$E_{\text{max}} := \max_{\mu \in \Xi_{\text{test}}} \frac{\|\mathbb{P}_{\text{pu}}[u_\mu^{\text{hf}}] - \mathbb{P}_{\text{pu}}[\widehat{u}_\mu]\|_{H^1(\Omega)}}{\|\mathbb{P}_{\text{pu}}[u_\mu^{\text{hf}}]\|_{H^1(\Omega)}}. \quad (41b)$$

As mentioned in section 3, we here resort to the HF CB solver to generate HF data for training and test, to simplify interpretation of the numerical results. In several figures, we compare the prediction error (41a) with the error associated with the mapped $H^1(\Omega_{L_i}^a)$ projection of $u_\mu^{\text{hf}} \circ \Phi_i$, for $i = 1, \dots, N_{\text{dd}}$,

$$E_{\text{avg}}^{\text{opt}} := \frac{1}{n_{\text{test}}} \sum_{\mu \in \Xi_{\text{test}}} \frac{\|\mathbb{P}_{\text{pu}}[u_\mu^{\text{hf}}] - \mathbb{P}_{\text{pu}}[\widehat{u}_\mu^{\text{opt}}]\|_{H^1(\Omega)}}{\|\mathbb{P}_{\text{pu}}[u_\mu^{\text{hf}}]\|_{H^1(\Omega)}}, \quad \text{with } (\widehat{u}_\mu^{\text{opt}})_i = \left(\Pi_{\mathcal{Z}_{L_i}^{\text{a,b}} \cup \mathcal{W}_{L_i}^{\text{a,p}}} u_\mu^{\text{hf}} \circ \Phi_i \right) \circ \Phi_i^{-1}, \quad (42)$$

for $i = 1, \dots, N_{\text{dd}}$. Note that (42) is not optimal — that is, it is not the relative $H^1(\Omega)$ projection error associated with the instantiated spaces — but it can be shown to be quasi-optimal exploiting [1, Theorem 1]. We omit the details.

We resort to a P2 FE discretization with $N_{\text{int}}^e = 1120$ and $N_{\text{ext}}^e = 3960$ elements, and $N_{\text{int}}^p = 272$ and $N_{\text{ext}}^p = 200$ port quadrature points. We emphasize that the HF component-based discretization is constructed to ensure that the local grids match exactly for $Q_a = Q_{\text{ref}}$ (cf. Figure 3); however, we remark that internal and external meshes do not lead to a global conforming discretization for any other value of Q_a .

All simulations are performed in Matlab 2020b on a commodity laptop. The implementation of the method does not resort to any parallelization of offline and online solves.

5.2 Reduced-order model with HF quadrature

We show the performance of the OS2 ROM without hyper-reduction. First, we show the behavior of the percentage of retained energy of the POD eigenvalues $\{\lambda_i\}_i$ of the Gramian matrix associated with the snapshot set. To facilitate visualization, we show the average in-sample error $E_n = 1 - \frac{\sum_{i=1}^n \lambda_i}{\sum_{j=1}^{n_{\text{train}}} \lambda_j}$ for several values of n , for port and bubble components, and for the two archetype components. We observe that the POD eigenvalues decay extremely rapidly, for both components.

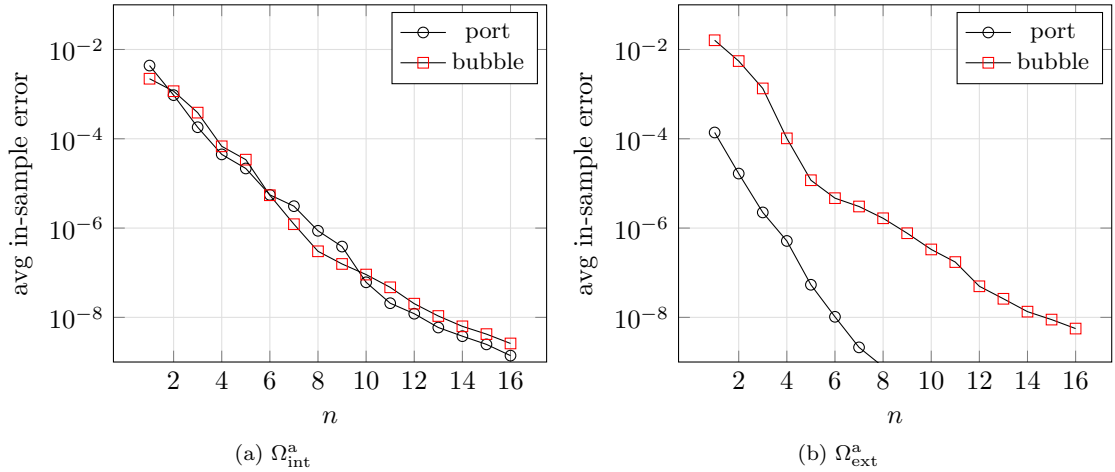


Figure 5: behavior of the average squared in-sample error $E_n = 1 - \frac{\sum_{i=1}^n \lambda_i}{\sum_{j=1}^{n_{\text{train}}} \lambda_j}$ for several values of n , for port and bubble components, and for the two archetype components.

In Figure 6, we compare the average error E_{avg} (41a) associated with the OS2 ROM for several values of m and $n = m$ and $n = 2m$, with the average error $E_{\text{avg}}^{\text{opt}}$ (42) obtained through projection. We observe that the OS2 ROM achieves near-optimal performance for all choices of the port and bubble ROBs. We also observe that doubling the number of port modes m by keeping the same number of bubble modes n does not lead to relevant differences in terms of both projection and OS2 prediction error. In the remainder, we set $m = n$.

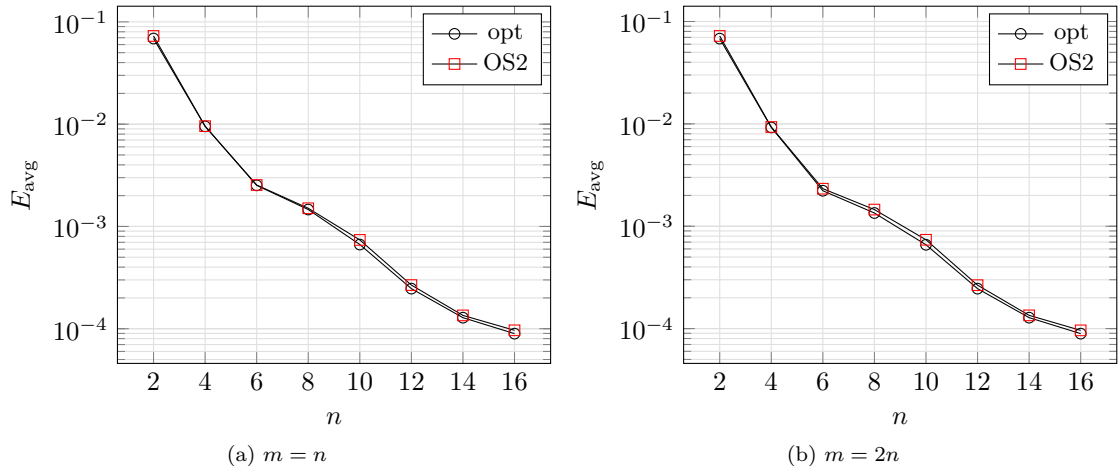


Figure 6: out-of-sample performance of OS2 ROM without hyper-reduction for several values of m , with $n = m$ and $n = 2m$; comparison with optimal (“opt”) average error $E_{\text{avg}}^{\text{opt}}$ (42)

Figure 7 shows the behavior of the solution over a vertical slice of the domain for a test configuration with $Q_a = 7$; boundaries of the Q_a internal subdomains associated with repositories and the external subdomain are marked as black dots in 7 (a); the vertical slice, drawn as a purple dashed line, corresponds to points (x, y) such that $x = \bar{x} = 0.43$, $0 \leq y \leq 1$. Points of the slice belong to either the instantiated component Ω_3 or Ω_8 (or both). We apply the partition of unity operator (40) to generate globally-defined solutions. We compute therefore approximate solutions $\mathbb{P}_{\text{pu}}[\hat{u}_*^{(n=2)}]$, $\mathbb{P}_{\text{pu}}[\hat{u}_*^{(n=10)}]$ corresponding to two choices of the ROB size $n = m = 2$ and $n = m = 10$ and for subscript \star corresponding to x and y components; we also compare the reduced solutions with the HF globally defined solutions $\mathbb{P}_{\text{pu}}[u_*^{\text{hf}}]$. We observe that the choice $n = m = 2$ enables qualitatively accurate approximations of the vertical displacement (cf. 7(c)), but extremely inaccurate approximations of the horizontal displacement (cf. Figure 7(b)), while the choice $n = m = 10$ leads to accurate predictions for both horizontal and vertical displacements.

5.3 Hyper-reduction of the port-to-bubble maps

Figure 8 investigates performance of the EQ rule for different tolerances tol_{eq} (cf. A): Figures 8(a) and 8(b) show the behavior of the out-of-sample relative error compared to the OS2 ROM with HF quadrature (dubbed HFQ); in Figure 8(a) we depict E_{avg} , in Figure 8(b) we depict E_{max} . Figures 8(c) and 8(d) show the percentage of sampled elements as a function of m , for the two archetype components and for several tolerances. We observe that for $tol_{\text{eq}} \leq 10^{-10}$ the hyper-reduced OS2 ROM is as accurate as the OS2 ROM with HF quadrature for all values of m considered. We further observe that the percentage of sampled elements is between three and five times larger in the internal component — since $N_{\text{ext}}^e \approx 3.5N_{\text{int}}^e$, we have that the absolute number of sampled elements is nearly the same for the two components.

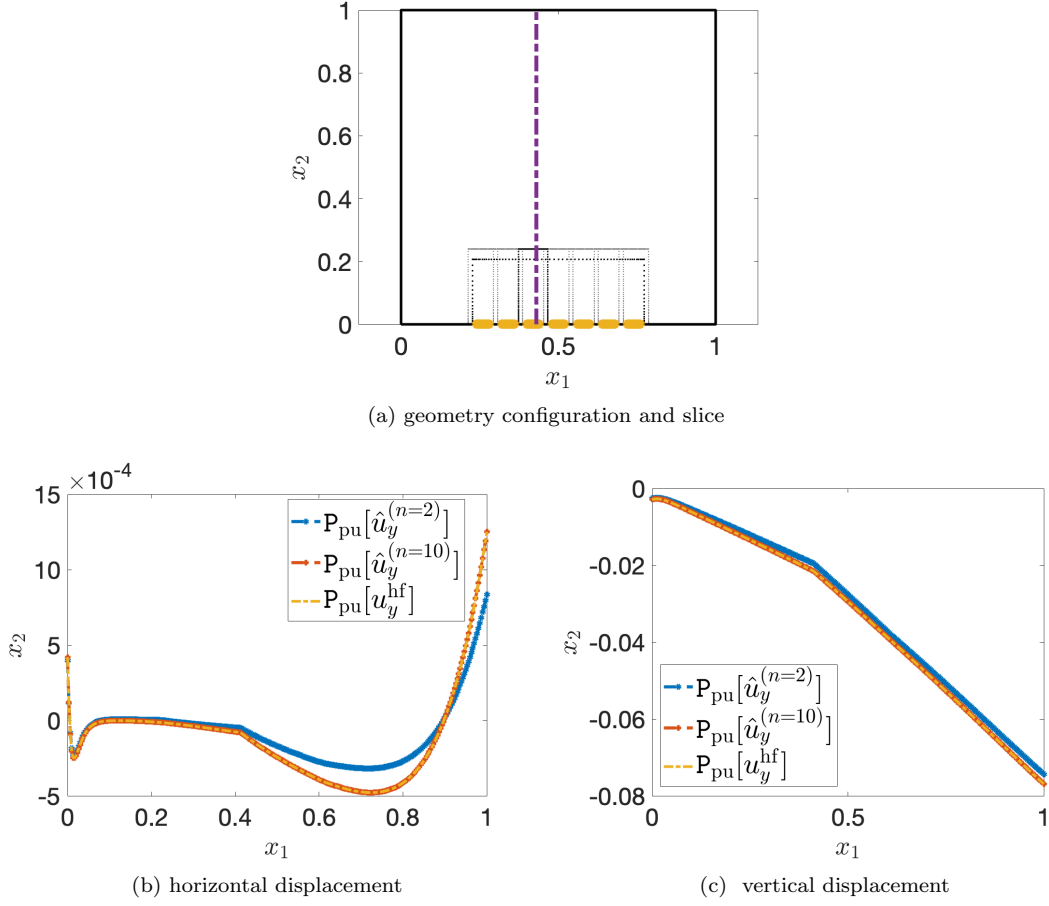


Figure 7: visualization of the horizontal and vertical displacement components for a vertical slice.

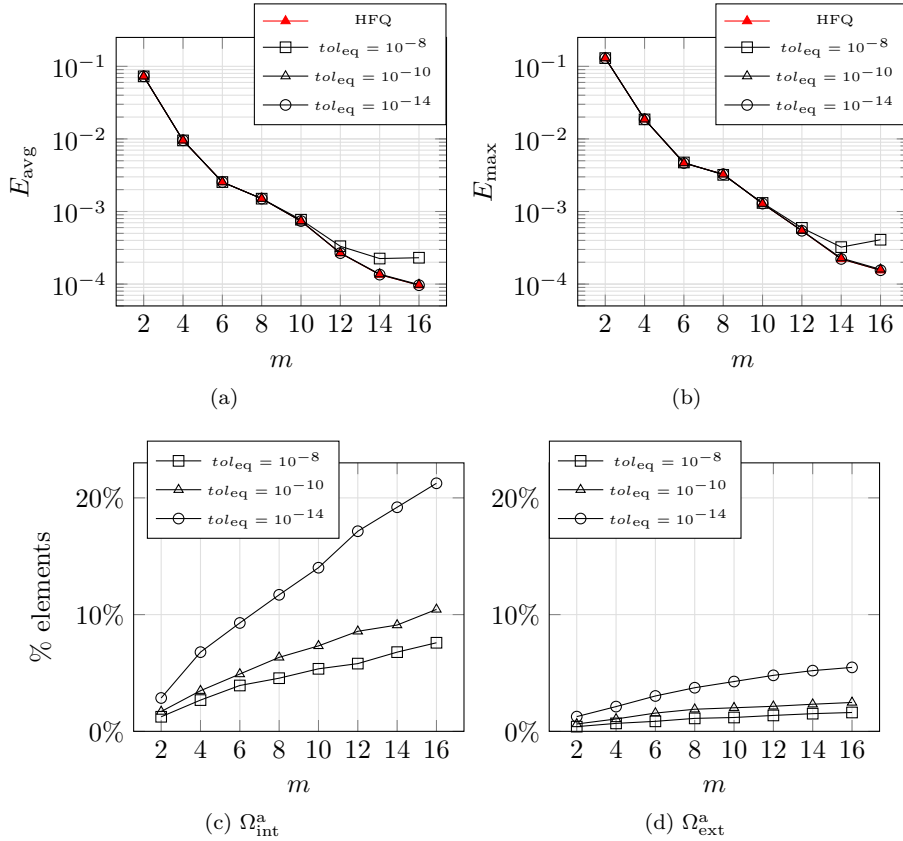


Figure 8: hyper-reduction of the port-to-bubble maps for several tolerances tol_{eq} and port space sizes m , with $n = m$. Behavior of the (a) average, (b) max out-of-sample prediction. (c)-(d) percentage of sampled elements in Ω_{int}^a and Ω_{ext}^a .

5.4 Hyper-reduction of the objective function

In Figure 9, we show the behavior of the L^∞ error

$$E_{\text{avg,eim}}^\infty(\ell, m) := \frac{1}{n_{\text{train},\ell}} \sum_{k=1}^{n_{\text{train},\ell}} \left\| u_{\ell,k}^p - \mathcal{G}_{\ell,m}[u_k^p] \right\|_\infty$$

where $\{u_{\ell,k}^p\}_{k=1}^{n_{\text{train},\ell}}$ are the port fields associated with the ℓ -th component and employed to generate the port basis (cf. Algorithm 2). We observe near-exponential convergence of the L^∞ error for both components; interestingly, the interpolation error for the internal component is one order of magnitude larger than the error for the external component.

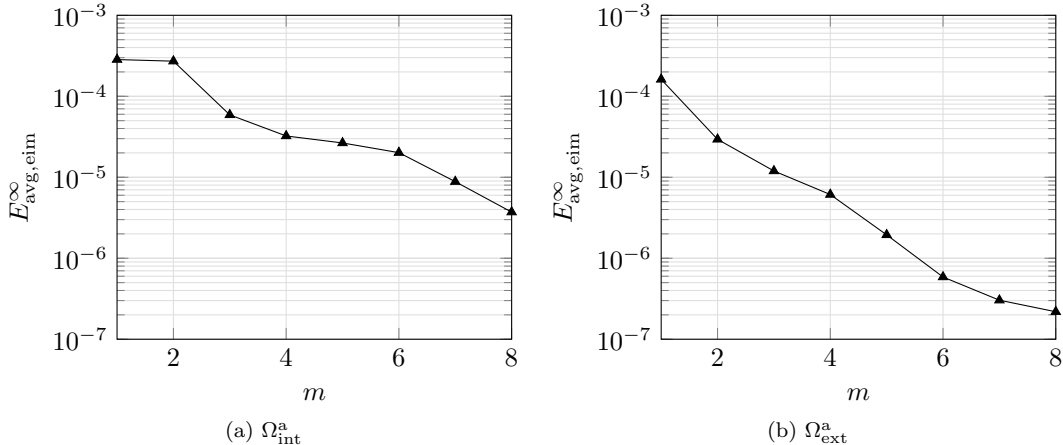


Figure 9: application of the EIM procedure for vector-valued fields (cf. Algorithm 3). (a)-(b) behavior of the in-sample L^∞ approximation error $E_{\text{avg,eim}}^\infty$ for the internal and the external component.

In Figure 10, we report the percentage of sampled quadrature points by the two hyper-reduction procedures. By construction, EIM selects $m_{\text{p,eq}} = m$ points; on the other hand, the number of points selected by the EQ procedure of section 3.3.1 weakly depends on the size m of the port basis.

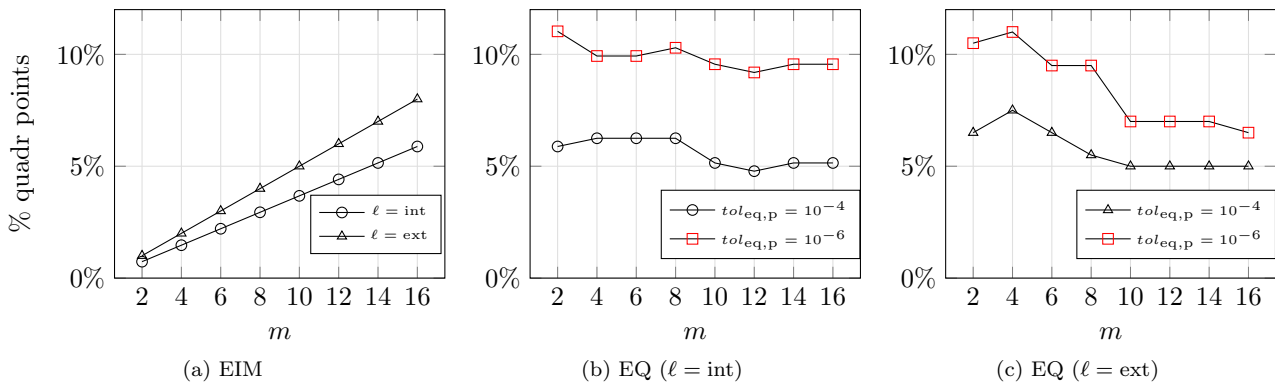


Figure 10: hyper-reduction of the objective function for internal and external archetype components, with respect to m , with $n = m$. (a) percentage of sampled quadrature points based on EIM. (b)-(c) percentage of sampled quadrature points based on the EQ procedure, for two tolerances $tol_{\text{eq,p}}$.

In Figure 11, we investigate the performance of the fully hyper-reduced ROM: Figure 11(a) shows the behavior of the prediction error (41a), while Figure 11(b) shows the behavior of the maximum wall-clock time over the test set. We observe that the speed-up due to hyper-reduction of the objective function is of the order 1.5 for all choices of m ; on the other hand, performance of the two considered hyper-reduction strategies is comparable for all tests. In Figure 11(c) the out-of-sample error distributions are depicted in the case without hyper-reduction on the objective function for different values of m .

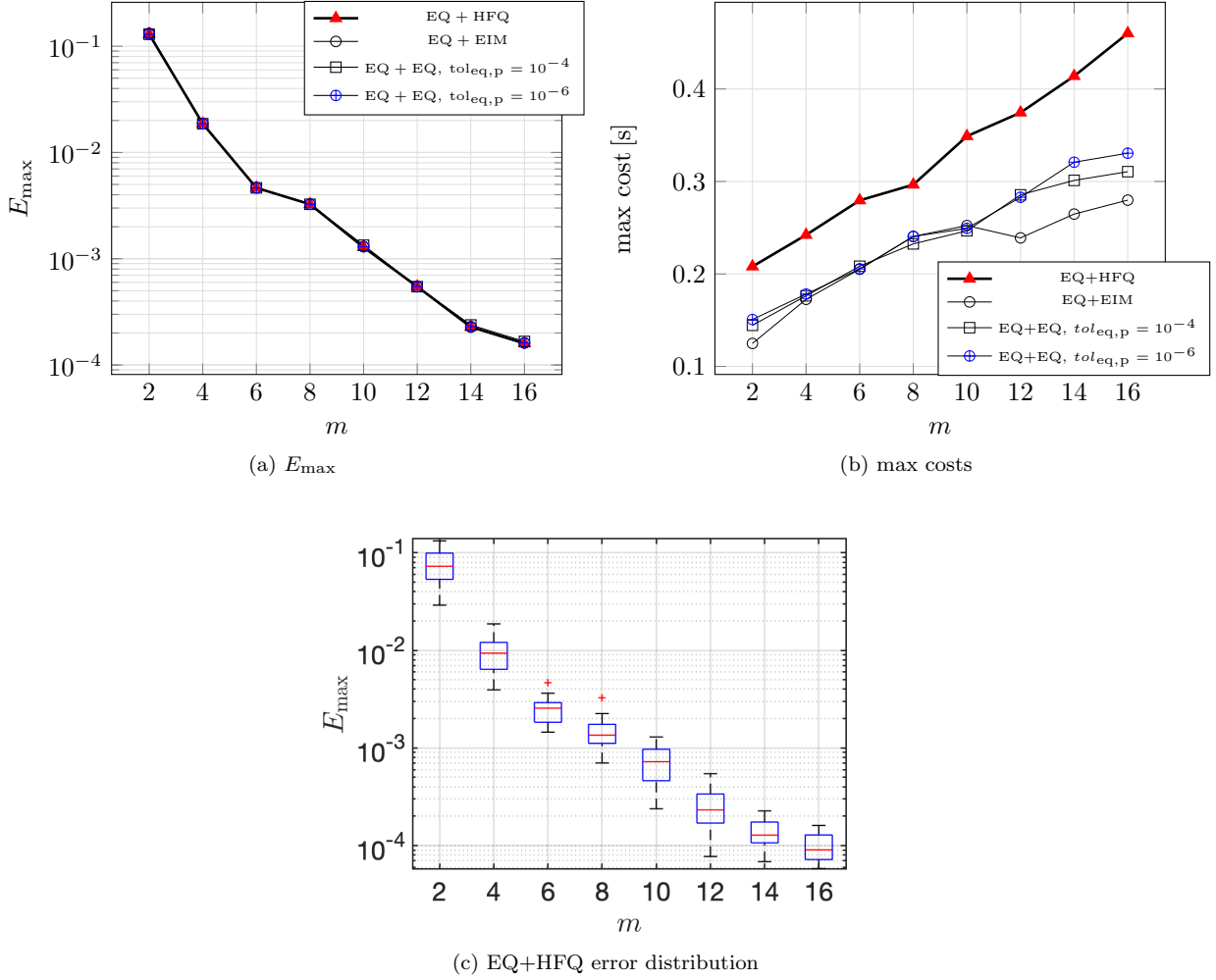


Figure 11: hyper-reduction of the objective function based on EIM and EQ. (a) worst out-of-sample performance of the hyper-reduced OS2 ROM for several choices of m , with $n = m$. (b) maximum computational cost over the test set. (c) Out-of-sample error distributions for the EQ+HFQ case. Results are based on the EQ tolerance $tol_{eq} = 10^{-10}$ for the local problems and the tolerances $tol_{eq,p} = 10^{-4}$ and $tol_{eq,p} = 10^{-6}$ for the objective function (for EQ+EQ).

In Figure 12 we show the speed-up factor of the hyper-reduced OS2 solvers with respect to a representative monolithic HF solver of comparable accuracy for different numbers of subdomains. The monolithic P2 FE solver runs in approximately³ 2.7806 [s] for $N_{dd} = 2$ and in 9.9971 [s] for $N_{dd} = 8$; the CB HF solver (10) that is used to generate training and test data is roughly a factor three slower than the corresponding monolithic solver. We define the speed-up factor as:

$$\text{speed-up}(N_{dd}) := \frac{t_{hf}(N_{dd})}{t_{OS2}(N_{dd})}$$

where t_{hf} is the estimated execution time of the monolithic HF solver averaged over 5 tests and t_{OS2} is the execution time associated with the CB ROM, averaged over the same 5 configurations, for $N_{dd} \in \{3, \dots, 8\}$. We perform hyper-reduction of the port-to-bubble maps using the tolerance $tol_{eq} = 10^{-10}$ and we consider the tolerances $tol_{eq,p} = 10^{-4}$ and $tol_{eq,p} = 10^{-6}$ for the hyper-reduction of the objective function (for the EQ+EQ case).

³Computational times are based on an average over 5 tests for each number of subdomains; the computational grid has 17177 FE nodes for $N_{dd} = 2$ and it has 38637 nodes for $N_{dd} = 8$.

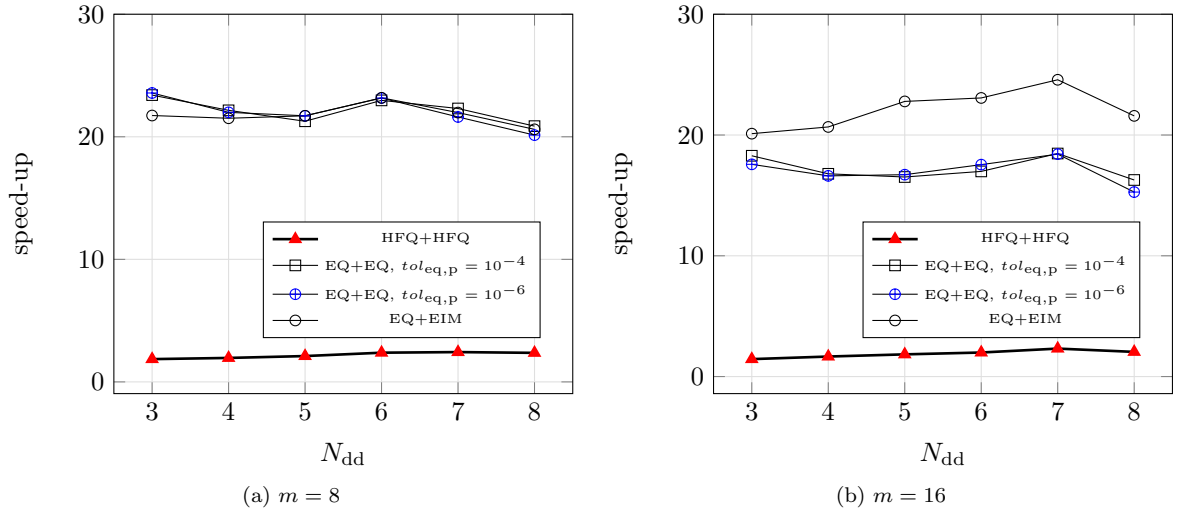


Figure 12: Speed-up of the OS2 ROMs with respect to the HF monolithic solver for several values of the number of subdomains. (a) performance for $m = 8$; (b) performance for $m = 16$. EQ tolerance for the port-to-bubble maps is set equal to $tol_{eq} = 10^{-10}$.

We observe that the speed-up factors depicted in Figure 12 depend weakly on the number of subdomains. The EIM method leads to slightly larger speed-ups than the EQ method for $m = n = 16$ (cf. Figure 12(b)), while performance is comparable for the case $m = n = 8$ (Figure 12(a)). We envision that more effective implementations of Algorithm 1 — which rely on parallelization of the port-to-bubble loop at Lines 4-7 and on pointwise EQ hyper-reduction of the port-to-bubble maps, as opposed to element-wise EQ — will lead to significantly larger speed-ups.

5.5 Optimization strategy: comparison between Gauss-Newton, quasi-Newton and overlapping Schwarz

We compare the performance of the Gauss-Newton method and the quasi-Newton method discussed in section 2.5 for various choices of m and $n = m$; to provide a concrete reference, we also consider the multiplicative overlapping Schwarz method with Dirichlet interface conditions. More precisely, we implement the iterative procedure described in Algorithm 4: note that the OS method simply requires the solution to a sequence of problems on the subdomains with information propagating through the boundary conditions; since the discretization is not conforming across components, we should define the i -th port mode using projection (cf. Line 5, Algorithm 4). Note that at step i of the for loop at Lines 4 – 7 we use the values of $\hat{\beta}_i, \dots, \hat{\beta}_{N_{dd}}$ at the previous iteration and the values $\hat{\beta}_1, \dots, \hat{\beta}_{i-1}$ at the current iteration: the for loop is thus not parallelizable. We set $tol = 10^{-6}$ in Algorithm 1 (cf. Line 11) and we consider the same termination criterion for the quasi-Newton solver and the OS solver. In this test, we perform hyper-reduction at the local level (EQ tolerance 10^{-10}), but we do not hyper-reduce the objective function.

Algorithm 4 Overlapping Schwarz method.

Inputs: $\boldsymbol{\alpha}^{(0)} = [\boldsymbol{\alpha}_1^{(0)}, \dots, \boldsymbol{\alpha}_{N_{\text{dd}}}^{(0)}]$, $\boldsymbol{\beta}^{(0)} = [\boldsymbol{\beta}_1^{(0)}, \dots, \boldsymbol{\beta}_{N_{\text{dd}}}^{(0)}]$ initial conditions (cf. Eq. (20)), $tol > 0, \text{maxit}$.

Outputs: $\widehat{\boldsymbol{\beta}}$ port coefficients, $\widehat{\boldsymbol{\alpha}} = \widehat{\mathbf{F}}^{\text{eq}}(\widehat{\boldsymbol{\beta}})$ bubble coefficients.

- 1: Set $\widehat{\boldsymbol{\beta}}^{(0)} = \boldsymbol{\beta}^{(0)}$ and $\widehat{\boldsymbol{\alpha}} = \boldsymbol{\alpha}^{(0)}$.
 - 2: **for** $k = 1, \dots, \text{maxit}$ **do**
 - 3: Initialize $\widehat{\boldsymbol{\alpha}}^{(k)} = \widehat{\boldsymbol{\alpha}}^{(k-1)}$ and $\widehat{\boldsymbol{\beta}}^{(k)} = \widehat{\boldsymbol{\beta}}^{(k-1)}$.
 - 4: **for** $i = 1, \dots, N_{\text{dd}}$ **do**
 - 5: Update $\widehat{\boldsymbol{\beta}}_i^{(k)} \in \arg \min_{\boldsymbol{\beta} \in \mathbb{R}^m} \sum_{j \in \text{Neigh}_i} \|W_i^{\text{p}} \boldsymbol{\beta} - Z_j^{\text{b}} \widehat{\mathbf{F}}_j^{\text{eq}}(\widehat{\boldsymbol{\beta}}_j^{(k)}) - W_j^{\text{p}} \widehat{\boldsymbol{\beta}}_j^{(k)}\|_{L^2(\Gamma_{i,j})}^2$.
 - 6: Update $\widehat{\boldsymbol{\alpha}}_i^{(k)} = \widehat{\mathbf{F}}_i^{\text{eq}}(\widehat{\boldsymbol{\beta}}_i^{(k)})$.
 - 7: **end for**
 - 8: **if** $\|\widehat{\boldsymbol{\beta}}^{(k)} - \widehat{\boldsymbol{\beta}}^{(k-1)}\|_2 < tol \|\widehat{\boldsymbol{\beta}}^{(k)}\|_2$ **then**, BREAK
 - 9: **end if**
 - 10: **end for**
-

Figure 13(a) shows the behavior of the objective function in (15) with respect to the ROB sizes over the test set, while Figure 13(b) shows the number of iterations required to meet the termination criterion: we observe that GNM requires many fewer iterations without any deterioration in accuracy. Figure 13(c) shows the wall-clock average cost for the three methods: even if GNM has a slightly larger per-iteration cost, we empirically find that OS2 with GNM is significantly more rapid than the other two approaches. Furthermore, since the OS internal loop (cf. Lines 4-7 Algorithm 4) is not parallelizable as opposed to the corresponding loop of the OS2 solver (cf. Lines 4-7 Algorithm 1), we expect significantly larger computational gains if we resort to parallel computing.

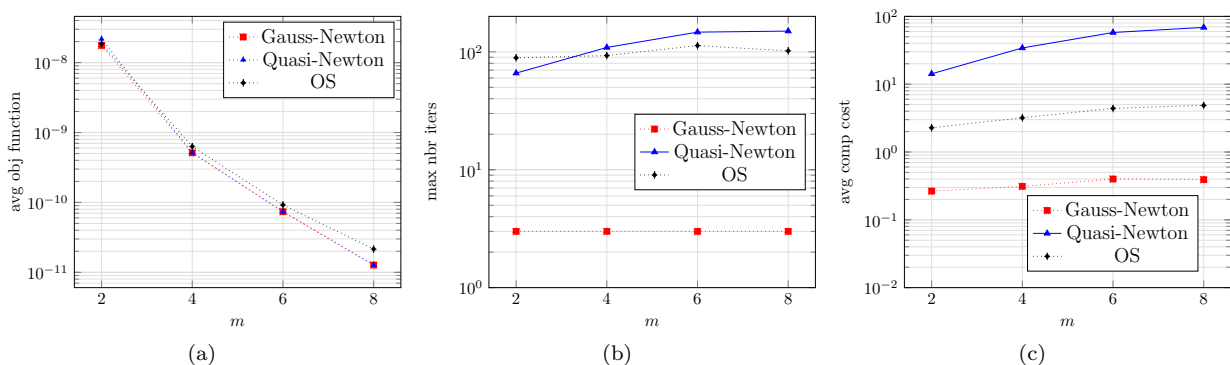


Figure 13: comparison between OS2 with Gauss-Newton optimization and with quasi-Newton optimization, and multiplicative overlapping Schwarz methods. (a) average value of the objective function with respect to m and for $n = m$. (b) maximum number of iterations to meet the convergence criterion. (c) average wall-clock cost with respect to m and for $n = m$.

In Figure 14, we repeat the test of Figure 13 for the choice of the initial conditions $\boldsymbol{\alpha}^{(0)} = \mathbf{0}$ and $\boldsymbol{\beta}^{(0)} = \mathbf{0}$ in Algorithm 1 and Algorithm 4. We observe that OS and OS2 with GNM show similar performance with respect to all metrics, while OS2 with QN, instead of converging to the optimal solution, converges to a different local minimum for two configurations for $m = 6$.

6 Conclusions

In this work we developed and numerically validated the one-shot overlapping Schwarz (OS2) approach to component-based MOR of steady nonlinear PDEs. The key features of the approach are (i) a constrained optimization statement that penalizes the jump at the components' interfaces subject to the approximate satisfaction of the PDE in each deployed (instantiated) component; (ii) the decomposition of the local solutions into a *port component* — associated with the solution on interior boundaries (*ports*) — and a *bubble component* that vanishes at *ports*, to enable effective parallelization of the online solver. Hyper-reduction of the local sub-problems and of the objective function is performed to reduce online assembly costs. We illustrate the

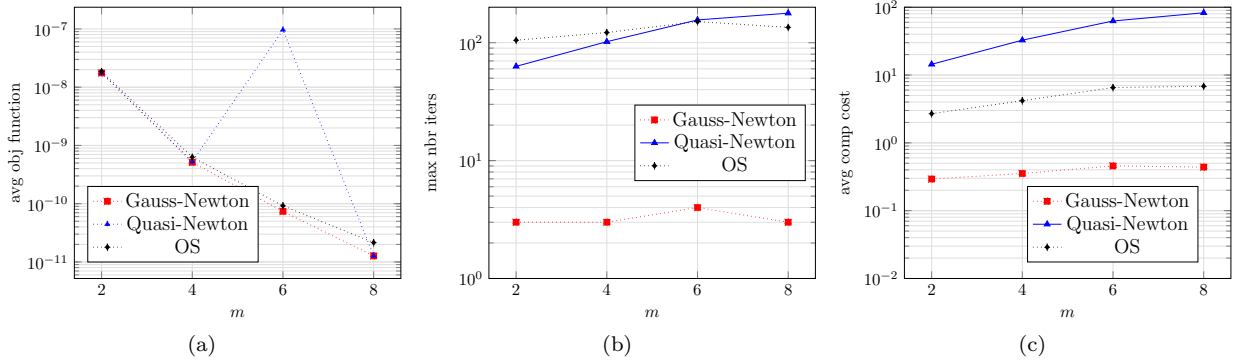


Figure 14: comparison between Gauss-Newton, quasi-Newton methods, and multiplicative overlapping Schwarz methods with zero initial condition. (a) average value of the objective function with respect to m and for $n = m$. (b) maximum number of iterations to meet the convergence criterion. (c) average wall-clock cost with respect to m and for $n = m$.

many elements of the formulation through the application to a two-dimensional nonlinear mechanics (Neo-Hookean) PDE model; for this problem, we are able to devise a CB-ROM that reduces online costs by a factor 20 compared to a standard monolithic FE model with less than 0.1% prediction error, and without resorting to any parallelization of the online ROM solver. We also observe that for the particular model problem considered in this paper the OS2 formulation provides acceptable results also for under-resolved ROB.

We aim to extend our approach in several directions. First, we wish to apply the OS2 method to more challenging problems in nonlinear mechanics, with particular emphasis on thermo-hydro-mechanical (THM) systems [32]: towards this end, we should extend the OS2 formulation to unsteady PDEs and we should also devise specialized routines to deal with internal variables. In this respect, we envision to combine our approach with the recently-developed OS method discussed in [44, 18, 3]. Second, we wish to devise localized training techniques to avoid the solution to global HF problems at training stage: in this regard, we aim to extend the approach in [54] to unsteady PDEs with internal variables. Third, we aim to combine data-fitted and projection-based ROMs in the OS2 framework: we envision that the successful combination of first-principle and data-fitted models might offer new solutions for data assimilation (state estimation) applications, for a broad range of engineering tasks. Fourth, we wish to investigate the possibility of generalizing our approach to non-overlapping decompositions: this requires to add in the objective function a term that penalizes the jump of the normal stresses; a deep investigation of the connection with discontinuous Galerkin methods should also be considered.

Acknowledgements

The authors acknowledge the financial support of Andra (National Agency for Radioactive Waste Management) and thank Dr. Marc Leconte and Dr. Antoine Pasteau (Andra) for fruitful discussions; The authors also thank Dr. Irina K. Tezaur (Sandia National Laboratories) for her pertinent and useful comments on this work. The authors acknowledge the support by European Union's Horizon 2020 research and innovation programme under the Marie Skłodowska-Curie Actions, grant agreement 872442 (ARIA).

A Hyper-reduction of port-to-bubble problems

We review the element-wise EQ hyper-reduction procedure that is employed here to speed up the solution to the port-to-bubble problems. The approach exploits the methods first proposed in [22, 63]: we refer to [57] for further details. We recall that, for any $\ell \in \mathcal{L}$, $\{x_{\ell,j}^{a,v}\}_{j=1}^{N_\ell^v}$ are the nodes of the reference mesh of the ℓ -th component, while $\mathbf{T}_\ell \in \mathbb{N}^{N_\ell^e \times n_{lp}}$ is the connectivity matrix, with n_{lp} equal to the number of elemental degrees of freedom. We denote by e_1, \dots, e_D the vectors of the canonical basis in \mathbb{R}^D and we denote by $\varphi_{\ell,k,i}$ the FE basis associated with the i -th degree of freedom of the k -th element of the ℓ -th component.

Given $u \in \mathcal{X}_\ell^a$, we denote by $\mathbf{u}^{\text{un}} \in \mathbb{R}^{n_{lp} \times N_\ell^e \times D}$ the corresponding third-order tensor such that

$$u_{i,k,d}^{\text{un}} = \left(u \left(x_{\ell, \mathbf{T}_\ell, k, i}^{a,v} \right) \right)_d, \quad i = 1, \dots, n_{lp}, \quad k = 1, \dots, N_\ell^e, \quad d = 1, \dots, D.$$

Similarly, given the ROB basis $Z_\ell^{a,b} : \mathbb{R}^n \rightarrow \mathcal{Z}_\ell^{a,b}$, we denote by $\mathbf{Z}_\ell^{a,b,\text{un}} \in \mathbb{R}^{n_{lp} \times N_\ell^e \times D \times n}$ the corresponding fourth-order tensor. We further define the unassembled residual associated with the field u and the parameter

μ_ℓ ,

$$R_{\ell,i,k,d}^{\text{a,un}}(u; \mu_\ell) := \int_{\mathbb{D}_{\ell,k}} \eta_\ell^{\text{a,e}}(u, \varphi_{\ell,k,i} e_d; \mu_\ell) dx + \int_{\partial \mathbb{D}_{\ell,k}} \eta_\ell^{\text{a,f}}(u, \varphi_{\ell,k,i} e_d; \mu_\ell) dx,$$

for $\ell \in \mathcal{L}$, $i = 1, \dots, n_{\text{ip}}$, $k = 1, \dots, N_\ell^e$, $d = 1, \dots, D$. Then, it is easy to verify that

$$\left(\widehat{\mathbf{R}}_\ell^\star(\gamma_\ell) \right)_j = \sum_{i,k,d} \rho_{\ell,k}^\star Z_{\ell,i,k,d,j}^{\text{a,b,un}} R_{\ell,i,k,d}^{\text{a,un}}(\gamma_\ell) = (\mathbf{G}_\ell^{\text{a}}(\gamma_\ell) \rho_\ell^\star)_j, \quad j = 1, \dots, n, \quad (43\text{a})$$

where $\star \in \{\text{hf}, \text{eq}\}$, $\gamma_\ell = (\boldsymbol{\alpha}_\ell, \boldsymbol{\beta}_\ell, \mu_\ell)$ denotes the triplet of bubble coefficients, port coefficients and parameter, $\mathbf{G}_\ell^{\text{a}} : \mathbb{R}^n \times \mathbb{R}^m \times \mathcal{P}_\ell \rightarrow \mathbb{R}^{n \times N_\ell^e}$ is the matrix-valued function that satisfies $(\mathbf{G}_\ell^{\text{a}}(\gamma_\ell))_{j,k} = \sum_{i,d} Z_{\ell,i,k,d,j}^{\text{a,b,un}} R_{\ell,i,k,d}^{\text{a,un}}(\gamma_\ell)$ for $j = 1, \dots, n$ and $k = 1, \dots, N_\ell^e$. The latter identity implies that

$$\widehat{\mathbf{R}}_\ell^{\text{hf}}(\gamma_\ell) - \widehat{\mathbf{R}}_\ell^{\text{eq}}(\gamma_\ell) = \mathbf{G}_\ell^{\text{a}}(\gamma_\ell) (\boldsymbol{\rho}_\ell^{\text{hf}} - \boldsymbol{\rho}_\ell^{\text{eq}}) \quad (43\text{b})$$

For any $\ell \in \mathcal{L}$, EQ procedures aim to find a vector $\boldsymbol{\rho}_\ell^{\text{eq}} \in \mathbb{R}^{N_\ell^e}$ such that (i) $\boldsymbol{\rho}_\ell^{\text{eq}}$ is as sparse as possible; (ii) the constant function is integrated accurately, that is

$$\left| \sum_{k=1}^{N_\ell^e} \rho_{\ell,k}^{\text{eq}} |\mathbb{D}_{\ell,k}| - |\Omega_\ell^{\text{a}}| \right| \ll 1; \quad (44)$$

(iii) given the training set of triplets $\Sigma_\ell^{\text{train,eq}} := \{\gamma_\ell^{(j)}\}_{j=1}^{n_{\text{train},\ell}}$, the residual is adequately calculated for all elements of the training set,

$$|\mathbf{J}_\ell^{\text{b}}(\gamma_\ell)^{-1} \left(\widehat{\mathbf{R}}_\ell^{\text{hf}}(\gamma_\ell) - \widehat{\mathbf{R}}_\ell^{\text{eq}}(\gamma_\ell) \right)| \ll 1, \quad \text{where } \mathbf{J}_\ell^{\text{b}} := \partial_{\boldsymbol{\alpha}} \widehat{\mathbf{R}}_\ell^{\text{hf}}, \quad \forall \gamma_\ell \in \Sigma_\ell^{\text{train,eq}}. \quad (45)$$

As discussed in section 3 (cf. (22)), the constant accuracy constraint (44) is designed to control the ℓ^1 norm of the weights that is related to the stability of the quadrature rule (see, e.g., [29, section 2.3]); the constraints (45) are directly linked to the approximation error between the ROM estimate with HF quadrature and the hyper-reduced ROM estimate (cf. [63, Proposition 3.2]).

We observe that the EQ problem can be recast as a sparse representation problem of the form

$$\min_{\boldsymbol{\rho} \in \mathbb{R}^{N_\ell^e}} \|\boldsymbol{\rho}\|_{\ell^0}, \quad \text{s. t.} \quad \|\mathbf{C}_\ell^{\text{eq}} (\boldsymbol{\rho}_\ell^{\text{hf}} - \boldsymbol{\rho}_\ell^{\text{eq}})\|_2 \leq \text{tol}_{\text{eq}}, \quad (46)$$

where $\|\boldsymbol{\rho}\|_{\ell^0}$ is the ℓ^0 norm that counts the number of non-zero entries in the vector $\boldsymbol{\rho}$, $\mathbf{C}_\ell^{\text{eq}}$ is a suitable matrix that can be readily derived from (44) and (45), and tol_{eq} is a suitable tolerance. Problem (46) is NP hard; however, several effective approximate strategies have been proposed in the literature to determine parsimonious quadrature rules for MOR applications, [22, 63, 12, 42]. In this work, we resort to the non-negative least-square algorithm implemented in the Matlab routine `lsqnonneg`, which takes as input the matrix $\mathbf{C}_\ell^{\text{eq}}$, the vector $\mathbf{b}_\ell^{\text{eq}} := \mathbf{C}_\ell^{\text{eq}} \boldsymbol{\rho}_\ell^{\text{hf}}$ and the tolerance tol_{eq} , and returns the sparse quadrature rule.

B Proofs

B.1 Proof of Theorem 4.1

Proof. Let u^\star be the solution to (24). Then, we find

$$a(u^\star|_{\Omega_i}, v) \stackrel{(25)}{=} a(u^\star, v^{\text{ext}}) = f(v^{\text{ext}}) = f(v) \quad \forall v \in \mathcal{X}_{i,0};$$

therefore, $u^\star|_{\Omega_i} = T_i u^\star|_{\Gamma_i} + G_i f$. The latter implies that $\lambda^\star = (u^\star|_{\Gamma_1}, u^\star|_{\Gamma_2})$ satisfies

$$\lambda^\star - E\lambda^\star - Gf = (u^\star|_{\Gamma_1} - u^\star|_{\Gamma_1}, u^\star|_{\Gamma_2} - u^\star|_{\Gamma_2}) = 0,$$

and thus that λ^\star solves (28).

Let λ^\star satisfy (28). We define $u_i^\star = T_i \lambda_i^\star + G_i f$ for $i = 1, 2$. If we define the space $\mathcal{X}_{1,2}^0 = \{v|_{\Omega_1 \cap \Omega_2} : v \in \mathcal{X}, v|_{\Gamma_1 \cup \Gamma_2} = 0\}$, we observe that u_1^\star, u_2^\star satisfy

$$u_i^\star|_{\Gamma_1} = \lambda_1^\star, \quad u_i^\star|_{\Gamma_2} = \lambda_2^\star, \quad a(u_i^\star, v) = f(v) \quad \forall v \in \mathcal{X}_{1,2}^0, \quad i = 1, 2. \quad (47)$$

Since $a : \mathcal{X}_{1,2}^0 \times \mathcal{X}_{1,2}^0 \rightarrow \mathbb{R}$ is coercive, the solution to (47) exists and is unique: therefore, $u_1^\star = u_2^\star$ in $\Omega_1 \cap \Omega_2$.

In particular, if we define $u^\star = \sum_{i=1}^2 u_i^\star$, we have $u^\star|_{\Omega_i} = u_i^\star$ for $i = 1, 2$.

Given $v \in \mathcal{X}$, we have $v\phi_i \in \mathcal{X}_{i,0}$, since, by construction, $\text{supp } \phi_i \subset \overline{\Omega}_i$. We thus have

$$a(u^\star, v) = \sum_{i=1}^2 a(u^\star, \phi_i v) = \sum_{i=1}^2 a(u^\star|_{\Omega_i}, \phi_i v) = \sum_{i=1}^2 a(u_i^\star, \phi_i v) = \sum_{i=1}^2 f(\phi_i v) = f(v),$$

which is the desired result. \square

B.2 Proof of Proposition 4.2

Proof. Continuity of a_p follows from the continuity of the trace operators, and the local operators T_1, T_2 . We omit the details. To prove inf-sup stability of the problem, we resort to the Fredholm's alternative: since T is compact, provided that $\nu = 1$ is not an eigenvalue of T , the equation $\lambda - T\lambda = f$ admits a unique solution for any $f \in \mathcal{U}$ and there exists a constant C such that $\|\lambda\| \leq C\|f\|$ (see, e.g., [51, Theorem 6.6.8]). It thus suffices to prove that $T\lambda = \lambda$ only holds for $\lambda = 0$.

Towards this end, we consider the problem:

$$\text{find } w \in \mathcal{X}_{1,2} : a(w, v) = 0 \quad \forall v \in \mathcal{X}_{1,2}^0, \quad w|_{\Gamma_1} = \gamma_1, \quad w|_{\Gamma_2} = \gamma_2,$$

with $\mathcal{X}_{1,2}^0 = \{v|_{\Omega_1 \cap \Omega_2} : v \in \mathcal{X}\}$, and $\mathcal{X}_{1,2}^0 = \{v|_{\Omega_1 \cap \Omega_2} : v \in \mathcal{X}, v|_{\Gamma_1 \cup \Gamma_2} = 0\}$. Since $T_1\lambda_1 = \lambda_1$ on Γ_1 by definition and $T_1\lambda_1 = \lambda_2$ on Γ_2 since $T\lambda = \lambda$, we have that $T_1\lambda_1|_{\Omega_{1,2}} = w$; similarly, we find $T_2\lambda_2|_{\Omega_{1,2}} = w$. As observed in the proof of Theorem 4.1, there exists a unique solution to the problem $w \in \mathcal{X}_{1,2}$: this implies that $T_1\lambda_1|_{\Omega_{1,2}} = T_2\lambda_2|_{\Omega_{1,2}}$. Given the partition of unity ϕ_1, ϕ_2 associated with $\{\Omega_i\}_{i=1}^2$, we define the field $u = \sum_{i=1}^2 \phi_i T_i \lambda_i \in \mathcal{X}$, which satisfies $u|_{\Omega_i} = T_i \lambda_i$ for $i = 1, 2$. We observe that

$$a(u, v) = \sum_{i=1}^2 a(u, \phi_i v) \stackrel{(25)}{=} \sum_{i=1}^2 a(u|_{\Omega_i}, \phi_i v) = \sum_{i=1}^2 a(T_i \lambda_i, \phi_i v) = 0.$$

Since a is coercive, we must have $u \equiv 0$ and thus $\lambda \equiv 0$. \square

B.3 Proofs of the estimate (34)

Proof. We first introduce the orthonormal basis $\{\psi_i\}_{i=1}^M$ of \mathcal{Z}^p ; given $\lambda \in \mathcal{Z}^p$, we denote by $\boldsymbol{\lambda} \in \mathbb{R}^M$ the corresponding vector of coefficients such that $\lambda = \sum_{i=1}^M (\boldsymbol{\lambda})_i \psi_i$. By straightforward calculations, we find that

$$\tilde{\mathbf{A}} \tilde{\boldsymbol{\lambda}} = \tilde{\mathbf{F}}, \quad \hat{\mathbf{A}} \hat{\boldsymbol{\lambda}} = \hat{\mathbf{F}}, \quad \text{with } \begin{cases} \left(\tilde{\mathbf{A}} \right)_{i,j} = \langle (Id - T)\psi_j, (Id - T)\psi_i \rangle, & \left(\tilde{\mathbf{F}} \right)_i = \langle (Id - T)\psi_i, Gf \rangle, \\ \left(\hat{\mathbf{A}} \right)_{i,j} = \langle (Id - \hat{T})\psi_j, (Id - \hat{T})\psi_i \rangle, & \left(\hat{\mathbf{F}} \right)_i = \langle (Id - \hat{T})\psi_i, \hat{G}f \rangle. \end{cases} \quad (48)$$

By straightforward calculations, we obtain

$$\tilde{\boldsymbol{\lambda}} - \hat{\boldsymbol{\lambda}} = \tilde{\mathbf{A}}^{-1} \left(\tilde{\mathbf{F}} - \hat{\mathbf{F}} - \left(\tilde{\mathbf{A}} - \hat{\mathbf{A}} \right) \hat{\boldsymbol{\lambda}} \right)$$

and thus

$$\|\tilde{\boldsymbol{\lambda}} - \hat{\boldsymbol{\lambda}}\|_2 \leq \underbrace{\|\tilde{\mathbf{A}}^{-1}\|_2}_{=: (I)} \left(\underbrace{\|\tilde{\mathbf{A}} - \hat{\mathbf{A}}\|_2}_{=: (II)} \underbrace{\|\hat{\boldsymbol{\lambda}}\|_2}_{=: (III)} + \underbrace{\|\tilde{\mathbf{F}} - \hat{\mathbf{F}}\|_2}_{=: (IV)} \right). \quad (49)$$

We estimate each term of (49) independently: combination of the estimates for (I)-(IV) leads to (34).

(I) Recalling the definition of α_p , we have $\|\psi - T\psi\| \geq \alpha_p \|\psi\|$; therefore, we have

$$\boldsymbol{\psi}^T \tilde{\mathbf{A}} \boldsymbol{\psi} = \|\psi - T\psi\|^2 \geq \alpha_p^2 \|\psi\|^2 = \alpha_p^2 \|\boldsymbol{\psi}\|_2^2,$$

which implies (I).

(II) By summing and subtracting $\langle (Id - T)\psi_j, (Id - \hat{T})\psi_i \rangle$ to $\left| \left(\tilde{\mathbf{A}} \right)_{i,j} - \left(\hat{\mathbf{A}} \right)_{i,j} \right|$ and recalling the definitions of $\gamma_p, \hat{\gamma}_p$ and ε_T , we obtain

$$\left| \left(\tilde{\mathbf{A}} \right)_{i,j} - \left(\hat{\mathbf{A}} \right)_{i,j} \right| \leq (\gamma_p + \hat{\gamma}_p) \varepsilon_T, \quad \forall i, j = 1, \dots, M.$$

Estimate (II) then follows by exploiting the fact that for any $M \times M$ matrix \mathbf{A} , we have $\|\mathbf{A}\|_2 \leq M \max_{i,j} |A_{i,j}|$.

(III) Estimate (III) follows directly from the properties of minimum residual formulations of inf-sup stable problems. Indeed, since the bilinear form a_p is continuous and inf-sup stable, using the Nečas theorem (see, e.g., [51, Thm 6.42]) we have $\|\hat{\boldsymbol{\lambda}}\|_2 = \|\hat{\boldsymbol{\lambda}}\| \leq \frac{1}{\alpha_p} \|\hat{G}f\|$ for all $f \in \mathcal{X}'$.

(IV) Proceeding as in (II), we find

$$\left| \left(\tilde{\mathbf{F}} \right)_i - \left(\hat{\mathbf{F}} \right)_i \right| \leq \hat{\gamma}_p \varepsilon_G + \|Gf\| \varepsilon_T, \quad \forall i = 1, \dots, M,$$

and thus $\|\tilde{\mathbf{F}} - \hat{\mathbf{F}}\|_2 \leq \sqrt{M} \|\tilde{\mathbf{F}} - \hat{\mathbf{F}}\|_\infty \leq \sqrt{M} (\hat{\gamma}_p \varepsilon_G + \|Gf\| \varepsilon_T)$. \square

B.4 Proof of (37)

Proof. For the two-subdomain problem, the OS2 statement (30) can be stated as:

$$\min_{(\psi_1, \psi_2) \in \mathcal{Z}_1^p \times \mathcal{Z}_2^p} \|\widehat{u}_1(\psi_1) - \widehat{u}_2(\psi_2)\|_{H^{1/2}(\Gamma_1 \cup \Gamma_2)} \quad (50)$$

where $\widehat{u}_i(\psi_i) = \widehat{u}_i^b(\psi_i) + E_i \psi_i$ and $\widehat{u}_i^b(\psi_i) \in \mathcal{Z}_i^b$ satisfies $a(\widehat{u}_i^b(\psi_i) + E_i \psi_i, v) = f(v)$ for all $v \in \mathcal{Z}_i^b$ and all $\psi_i \in \mathcal{Z}_i^p$, for $i = 1, 2$. If we differentiate (50), we obtain the optimality conditions

$$\begin{aligned} & (\widehat{u}_1^p - \chi_{\Gamma_1} (\widehat{u}_2^b(\widehat{u}_2^p) + E_2 \widehat{u}_2^p), \psi_1 - \chi_{\Gamma_1} (\widehat{u}_2^b(\psi_2) + E_2 \psi_2))_{H^{1/2}(\Gamma_1)} \\ & + (\widehat{u}_2^p - \chi_{\Gamma_2} (\widehat{u}_1^b(\widehat{u}_1^p) + E_1 \widehat{u}_1^p), \psi_2 - \chi_{\Gamma_2} (\widehat{u}_1^b(\psi_1) + E_1 \psi_1))_{H^{1/2}(\Gamma_2)} = 0 \quad \forall \psi = (\psi_1, \psi_2) \in \mathcal{Z}_1^p \times \mathcal{Z}_2^p, \end{aligned}$$

which can be rewritten as in (37). \square

B.5 Proofs of the estimates in section 4.5

In the following, we use the Taylor expansions:

$$e^x \sim 1 + x + x^2, \quad \frac{1}{1-x} \sim 1 + x + x^2, \quad (1+x)^{1/2} \sim 1 + \frac{1}{2}x - \frac{1}{8}x^2, \quad (1+x)^2 \sim 1 + 2x, \quad (51)$$

which are valid for $|x| \ll 1$. We further employ the identity:

$$\max\{|1 - \sigma\lambda_1|, |1 - \sigma\lambda_2|\} = \begin{cases} 1 - \sigma\lambda_1 & \sigma < \frac{2}{\lambda_1 + \lambda_2} \\ \sigma\lambda_2 - 1 & \sigma \geq \frac{2}{\lambda_1 + \lambda_2} \end{cases} \quad (52)$$

that is valid for any $0 \leq \lambda_1 \leq \lambda_2$.

B.5.1 Problem (38a)

It is easy to verify that the local solutions $\widehat{u}_1, \widehat{u}_2$ satisfy

$$\widehat{u}_1(x, \beta) = x^2 - \frac{\delta^2}{1+\delta}(1+x) + \frac{\beta}{1+\delta}(1+x), \quad \widehat{u}_2(x, \beta) = x^2 - \frac{\delta^2}{1+\delta}(1-x) + \frac{\beta}{1+\delta}(1+x). \quad (53)$$

By imposing $\beta_1 = \widehat{u}_2(\delta, \beta_2)$ and $\beta_2 = \widehat{u}_1(\delta, \beta_1)$ we obtain the system of equations:

$$\mathbf{A}_\delta \boldsymbol{\beta} = \mathbf{F}_\delta, \quad \text{with } \mathbf{A}_\delta = \begin{bmatrix} 1 & -c_\delta \\ -c_\delta & 1 \end{bmatrix}, \quad \mathbf{F}_\delta = \begin{bmatrix} d_\delta \\ d_\delta \end{bmatrix},$$

and $c_\delta = \frac{1-\delta}{1+\delta}$, $d_\delta = \frac{2\delta^3}{1+\delta}$. The matrix \mathbf{A}_δ is symmetric with positive eigenvalues $1 - c_\delta$ and $1 + c_\delta$; we thus have

$$\text{cond}(\mathbf{A}_\delta) = \frac{1+c_\delta}{1-c_\delta} = \frac{1}{\delta}, \quad \alpha_p = 1 - c_\delta = \frac{2\delta}{1+\delta}, \quad \gamma_p = 1 + c_\delta = \frac{2}{1+\delta}.$$

which are (39b) and (39c).

Multiplicative OS corresponds to the application of the Gauss-Seidel iterative method to the linear system $\mathbf{A}_\delta \boldsymbol{\beta} = \mathbf{F}_\delta$. We thus find

$$\boldsymbol{\beta}^{(k)} = \mathbf{P}_\delta^{\text{os}} \boldsymbol{\beta}^{(k-1)} + \mathbf{F}_\delta^{\text{os}}, \quad \text{with } \mathbf{P}_\delta^{\text{os}} = \begin{bmatrix} 0 & c_\delta \\ 0 & c_\delta^2 \end{bmatrix}, \quad \mathbf{F}_\delta^{\text{os}} = \begin{bmatrix} d_\delta \\ d_\delta + c_\delta d_\delta \end{bmatrix}.$$

We can then verify that the spectral radius of $\mathbf{P}_\delta^{\text{os}}$ is equal to

$$\rho_\delta^{\text{os}} = c_\delta^2 \sim 1 - 4\delta.$$

The OS2 method for (38a) reads as

$$\min_{\boldsymbol{\beta} \in \mathbb{R}^2} \frac{1}{2} \sum_{x \in \{-\delta, \delta\}} (\widehat{u}_1(x, \beta_1) - \widehat{u}_2(x, \beta_2))^2 = \frac{1}{2} \|\mathbf{A}_\delta \boldsymbol{\beta} - \mathbf{F}_\delta\|_2^2. \quad (54)$$

If we apply the gradient descent method to (54), we obtain

$$\boldsymbol{\beta}^{(k)} = (\mathbb{1} - \sigma \mathbf{A}_\delta^T \mathbf{A}_\delta) \boldsymbol{\beta}^{(k-1)} + \sigma \mathbf{A}_\delta^T \mathbf{F}_\delta.$$

By tedious calculations, we can verify that the eigenvalues of the transition matrix $\mathbb{1} - \sigma \mathbf{A}_\delta^T \mathbf{A}_\delta$ are equal to $1 - \sigma(c_\delta + 1)^2$ and $1 - \sigma(c_\delta - 1)^2$: recalling (52), we find that the spectral radius of the transition matrix is minimized by $\sigma = \frac{1}{c_\delta^2 + 1}$ and is equal to

$$\rho_\delta^{\text{os}2} = \frac{2c_\delta}{c_\delta^2 + 1} \sim 1 - 4\delta^2.$$

B.5.2 Problem (38b)

The local solutions \hat{u}_1, \hat{u}_2 satisfy

$$\hat{u}_1(x, \beta) = \beta \frac{e^{\gamma x} - e^{-\gamma}}{e^{\gamma\delta} - e^{-\gamma}}, \quad \hat{u}_2(x, \beta) = \frac{e^{\gamma x} - e^{-\gamma\delta}}{e^{\gamma} - e^{-\gamma\delta}} + \beta \frac{e^{\gamma} - e^{\gamma x}}{e^{\gamma} - e^{-\gamma\delta}}. \quad (55)$$

Exploiting the Taylor expansions in (51), we obtain

$$\hat{u}_1(-\delta, \beta) \sim \beta (1 - 2c_\gamma\delta + 2c_\gamma^2\delta^2), \quad \hat{u}_2(\delta, \beta) \sim 2d_\gamma\delta - 2d_\gamma^2\delta^2 + \beta (1 - 2d_\gamma\delta + 2d_\gamma^2\delta^2)$$

where $c_\gamma := \frac{\gamma}{1-e^{-\gamma}}$ and $d_\gamma := \frac{c_\gamma}{e^\gamma}$. We thus find the (approximate) system of equations

$$\mathbf{A}_\delta \boldsymbol{\beta} = \mathbf{F}_\delta, \quad \text{with } \mathbf{A}_\delta = \begin{bmatrix} 1 & (-1 + 2d_\gamma\delta - 2d_\gamma^2\delta^2) \\ (-1 + 2c_\gamma\delta - 2c_\gamma^2\delta^2) & 1 \end{bmatrix}, \quad \mathbf{F}_\delta = \begin{bmatrix} 2d_\gamma\delta - 2d_\gamma^2\delta^2 \\ 0 \end{bmatrix}.$$

Therefore, the Gauss-Seidel transition matrix is approximately equal to

$$\mathbf{P}_\delta^{\text{os}} \sim \begin{bmatrix} 0 & -1 + 2d_\gamma\delta \\ 0 & -(1 - 2d_\gamma\delta)(1 - 2c_\gamma\delta) \end{bmatrix}$$

and thus

$$\rho_\delta^{\text{os}} \sim 1 - 2(c_\gamma + d_\gamma)\delta = 1 - 2\frac{e^\gamma + 1}{e^\gamma - 1}\gamma\delta.$$

On the other hand, the eigenvalues of $\mathbf{A}_\delta^T \mathbf{A}_\delta$ are approximately equal to

$$\lambda_1 \sim \frac{(c_\gamma + 2d_\gamma)^2}{4}\delta^2, \quad \lambda_2 \sim 4 - (2c_\gamma + 4d_\gamma)\delta,$$

and thus

$$\alpha_p = \sqrt{\lambda_1} \sim \frac{4(e^\gamma + 2)\gamma\delta}{2(e^\gamma - 1)}, \quad \gamma_p = \sqrt{\lambda_2} \sim 2.$$

Exploiting (52), we find that the approximately optimal choice of the step size σ is equal to $\sigma = \frac{1}{2}(1 + (\frac{c_\gamma}{2} + d_\gamma)\delta)$ and thus

$$\rho_\delta^{\text{os}2} \sim 1 - \sigma\lambda_1 \sim 1 - \frac{1}{8}(c_\gamma + 2d_\gamma)^2\delta^2.$$

On the other hand, we obtain that the condition number of \mathbf{A}_δ is given by

$$\text{cond}(\mathbf{A}_\delta) = \sqrt{\frac{\lambda_{\max}(\mathbf{A}_\delta^T \mathbf{A}_\delta)}{\lambda_{\min}(\mathbf{A}_\delta^T \mathbf{A}_\delta)}} \sim \frac{\sqrt{4 - (2c_\gamma + 4d_\gamma)\delta}}{\frac{(c_\gamma + 2d_\gamma)}{2}\delta} \sim \frac{4}{(c_\gamma + 2d_\gamma)\delta} = \frac{4(e^\gamma - 1)}{4(e^\gamma + 2)\gamma\delta}$$

References

- [1] I. Babuška and J. M. Melenk. The partition of unity method. *International journal for numerical methods in engineering*, 40(4):727–758, 1997.
- [2] J. Baiges, R. Codina, and S. Idelsohn. A domain decomposition strategy for reduced order models. Application to the incompressible Navier–Stokes equations. *Computer Methods in Applied Mechanics and Engineering*, 267:23–42, 2013.
- [3] J. Barnett, I. Tezaur, and A. Mota. The schwarz alternating method for the seamless coupling of nonlinear reduced order models and full order models. *arXiv preprint arXiv:2210.12551*, 2022.
- [4] M. Barrault, Y. Maday, N. Nguyen, and A. Patera. An ‘empirical interpolation’ method: application to efficient reduced-basis discretization of partial differential equations. *C. R. Math. Acad. Sci. Paris Series I*, 339:667–672, 2004.
- [5] A. Benaceur and A. Patera. Port-reduced reduced-basis component method for steady state navier–stokes and passive scalar equations. Technical report, MIT, 2022.
- [6] M. Bergmann, A. Ferrero, A. Iollo, E. Lombardi, A. Scardigli, and H. Telib. A zonal Galerkin-free POD model for incompressible flows. *Journal of Computational Physics*, 352:301–325, 2018.
- [7] P. B. Bochev and D. Ridzal. An optimization-based approach for the design of PDE solution algorithms. *SIAM journal on numerical analysis*, 47(5):3938–3955, 2009.
- [8] M. Buffoni, H. Telib, and A. Iollo. Iterative methods for model reduction by domain decomposition. *Computers & Fluids*, 38:1160–1167, 2009.
- [9] A. Buhr, L. Iapichino, M. Ohlberger, S. Rave, F. Schindler, and K. Smetana. *Localized model reduction for parameterized problems*, pages 245–306. De Gruyter, 2020.
- [10] K. Carlberg, C. Farhat, J. Cortial, and D. Amsellem. The GNAT method for nonlinear model reduction: effective implementation and application to computational fluid dynamics and turbulent flows. *Journal of Computational Physics*, 242:623–647, 2013.

- [11] T. F. Chan, T. Y. Hou, and P.-L. Lions. Geometry related convergence results for domain decomposition algorithms. *SIAM Journal on Numerical Analysis*, 28(2):378–391, 1991.
- [12] T. Chapman, P. Avery, P. Collins, and C. Farhat. Accelerated mesh sampling for the hyper reduction of nonlinear computational models. *International Journal for Numerical Methods in Engineering*, 109(12):1623–1654, 2017.
- [13] S. Chen, Z. Ding, Q. Li, and S. J. Wright. A reduced order schwarz method for nonlinear multiscale elliptic equations based on two-layer neural networks. *arXiv preprint arXiv:2111.02280*, 2021.
- [14] Y. Chen, S. Cottlieb, L. Ji, and Y. Maday. An EIM-degradation free reduced basis method via over collocation and residual hyper reduction-based error estimation. *Journal of Computational Physics*, 444, 2021.
- [15] G. Ciaramella and M. J. Gander. Analysis of the parallel schwarz method for growing chains of fixed-sized subdomains: Part I. *SIAM Journal on Numerical Analysis*, 55(3):1330–1356, 2017.
- [16] D. Cinquegrana, R. Donelli, and A. Viviani. A hybrid method based on POD and domain decomposition to compute the 2-d aerodynamics flow field. *AIMETA, Bologna, Italy*, pages 1–10, 2011.
- [17] A. Corigliano, M. Dossi, and S. Mariani. Model order reduction and domain decomposition strategies for the solution of the dynamic elastic-plastic structural problem. *Computer Methods in Applied Mechanics and Engineering*, 290:127–155, 2015.
- [18] A. de Castro, P. Kuberry, I. Tezaur, and P. Bochev. A novel partitioned approach for reduced order model-finite element model (rom-fem) and rom-rom coupling. *arXiv preprint arXiv:2206.04736*, 2022.
- [19] L. Delves and C. Hall. An implicit matching principle for global element calculations. *IMA Journal of Applied Mathematics*, 23:223–234, 1979.
- [20] E. Du and M. Yano. Efficient hyperreduction of high-order discontinuous galerkin methods: element-wise and point-wise reduced quadrature formulations. *Journal of Computational Physics*, page 111399, 2022.
- [21] M. D’Elia and P. B. Bochev. Optimization-based coupling of nonlocal and local diffusion models. *MRS Online Proceedings Library (OPL)*, 1753, 2015.
- [22] C. Farhat, T. Chapman, and P. Avery. Structure-preserving, stability, and accuracy properties of the energy-conserving sampling and weighting method for the hyper reduction of nonlinear finite element dynamic models. *International journal for numerical methods in engineering*, 102(5):1077–1110, 2015.
- [23] C. Farhat, S. Grimberg, A. Manzoni, and A. Quarteroni. Computational bottlenecks for PROMs: Pre-computation and hyperreduction. *Handbook on Model Order Reduction. Volume 2: Snapshot-Based Methods and Algorithms. De Gruyter*, 2:181–244, 2021.
- [24] M. D. Gunzburger, J. S. Peterson, and J. N. Shadid. Reduced-order modeling of time-dependent PDEs with multiple parameters in the boundary data. *Computer methods in applied mechanics and engineering*, 196(4-6):1030–1047, 2007.
- [25] B. Haasdonk. Reduced basis methods for parametrized PDEs – a tutorial. In P. Benner, A. Cohen, M. Ohlberger, and K. Willcox, editors, *Model Reduction and Approximation*, pages 65–136. SIAM, Philadelphia, PA, 2017.
- [26] R. Herzog and K. Kunisch. Algorithms for PDE-constrained optimization. *GAMM-Mitteilungen*, 33(2):163–176, 2010.
- [27] J. Hesthaven, G. Rozza, and B. Stamm. *Certified reduced basis methods for parametrized partial differential equations*. Springer Briefs in Mathematics. Springer, Cham, 2016.
- [28] C. Hoang, Y. Choi, and K. Carlberg. Domain-decomposition least-squares petrov-galerkin (DD-LSPG) nonlinear model reduction. *Computer Methods in Applied Mechanics and Engineering*, 384:113997, 2021.
- [29] D. Huybrechs. Stable high-order quadrature rules with equidistant points. *Journal of computational and applied mathematics*, 231(2):933–947, 2009.
- [30] D. B. P. Huynh, D. J. Knezevic, and A. T. Patera. A static condensation reduced basis element method: approximation and a posteriori error estimation. *ESAIM Math. Model. Numer. Anal.*, 47(1):213–251, 2013.
- [31] L. Iapichino, A. Quarteroni, and G. Rozza. Reduced basis method and domain decomposition for elliptic problems in networks and complex parametrized geometries. *Computers & Mathematics with Applications*, 71(1):408–430, 2016.
- [32] A. Iollo, G. Sambataro, and T. Taddei. An adaptive projection-based model reduction method for nonlinear mechanics with internal variables: Application to thermo-hydro-mechanical systems. *International Journal for Numerical Methods in Engineering*, 123(12):2894–2918, 2022.
- [33] S. Kaulmann, M. Ohlberger, and B. Haasdonk. A new local reduced basis discontinuous galerkin approach for heterogeneous multiscale problems. *Comptes Rendus Mathématique*, 349(23-24):1233–1238, 2011.
- [34] P. Kerfriden, O. Goury, T. Rabczuk, and S. P.-A. Bordas. A partitioned model order reduction approach to rationalise computational expenses in nonlinear fracture mechanics. *Computer methods in applied mechanics and engineering*, 256:169–188, 2013.
- [35] C. L. Lawson and R. J. Hanson. *Solving least squares problems*, volume 161. Siam, 1974.
- [36] P. LeGresley and J. Alonso. Dynamic domain decomposition and error correction for reduced order models. In *41st Aerospace Sciences Meeting and Exhibit*, page 250, 2003.
- [37] K. Li, K. Tang, T. Wu, and Q. Liao. D3M: A deep domain decomposition method for partial differential equations. *IEEE Access*, 8:5283–5294, 2019.
- [38] P.-L. Lions. On the schwarz alternating method. I. In *First international symposium on domain decomposition methods for partial differential equations*, volume 1, page 42. Paris, France, 1988.
- [39] D. Lucia, P. King, M. Oxley, and P. Beran. Reduced order modeling for a one-dimensional nozzle flow with moving shocks. In *15th AIAA computational fluid dynamics conference*, page 2602, 2001.
- [40] Y. Maday, A. T. Patera, J. D. Penn, and M. Yano. A parameterized-background data-weak approach to variational data assimilation: formulation, analysis, and application to acoustics. *International Journal for Numerical Methods in Engineering*, 102(5):933–965, 2015.
- [41] K. Madsen, H. Nielsen, and O. Tingleff. *Methods for non-linear least square problems*. Department of Informatics and Mathematical Modelling, Technical University of Denmark, 2004.

- [42] M. Manucci, J. V. Aguado, and D. Borzacchiello. Sparse data-driven quadrature rules via ℓ^p -quasi-norm minimization. *Computational Methods in Applied Mathematics*, 22(2):389–411, 2022.
- [43] S. McBane and Y. Choi. Component-wise reduced order model lattice-type structure design. *Computer methods in applied mechanics and engineering*, 381:113813, 2021.
- [44] A. Mota, I. Tezaur, and G. Phlipot. The schwarz alternating method for transient solid dynamic. *International Journal for Numerical Methods in Engineering*, in press, 2022.
- [45] J. Nocedal and S. J. Wright. *Numerical optimization*. Springer, 2006.
- [46] L. Pegolotti, M. R. Pfaller, A. L. Marsden, and S. Deparis. Model order reduction of flow based on a modular geometrical approximation of blood vessels. *Computer Methods in Applied Mechanics and Engineering*, 380:113762, 2021.
- [47] A. Quarteroni, A. Manzoni, and F. Negri. *Reduced Basis Methods for Partial Differential Equations*. La Matematica per il 3+2. Springer International Publishing, 2016.
- [48] A. Quarteroni and A. Valli. *Domain decomposition methods for partial differential equations*. Number BOOK. Oxford University Press, 1999.
- [49] A. Radermacher and S. Reese. Model reduction in elastoplasticity: proper orthogonal decomposition combined with adaptive sub-structuring. *Computational Mechanics*, 54(3):677–687, 2014.
- [50] S. Riffaud, M. Bergmann, C. Farhat, S. Grimberg, and A. Iollo. The DGDD method for reduced-order modeling of conservation laws. *Journal of Computational Physics*, 437:110336, 2021.
- [51] S. Salsa. *Partial differential equations in action: from modelling to theory*, volume 99. Springer, 2016.
- [52] L. Sirovich. Turbulence and the dynamics of coherent structures. I. Coherent structures. *Quart. Appl. Math.*, 45(3):561–571, 1987.
- [53] K. Smetana and A. T. Patera. Optimal local approximation spaces for component-based static condensation procedures. *SIAM J. Sci. Comput.*, 38(5):A3318–A3356, 2016.
- [54] K. Smetana and T. Taddei. Localized model reduction for nonlinear elliptic partial differential equations: localized training, partition of unity, and adaptive enrichment. *arXiv preprint arXiv:2202.09872*, 2022.
- [55] T. Taddei. *Model order reduction methods for data assimilation; state estimation and structural health monitoring*. PhD thesis, Massachusetts Institute of Technology, 2017.
- [56] T. Taddei. An offline/online procedure for dual norm calculations of parameterized functionals: empirical quadrature and empirical test spaces. *Advances in Computational Mathematics*, 45(5):2429–2462, 2019.
- [57] T. Taddei and L. Zhang. A discretize-then-map approach for the treatment of parameterized geometries in model order reduction. *Computer Methods in Applied Mechanics and Engineering*, 384:113956, 2021.
- [58] S. Volkwein. Model reduction using proper orthogonal decomposition. *Lecture Notes, Institute of Mathematics and Scientific Computing, University of Graz*. see <http://www.uni-graz.at/imawww/volkwein/POD.pdf>, 1025, 2011.
- [59] M. Wicke, M. Stanton, and A. Treuille. Modular bases for fluid dynamics. *ACM Transactions on Graphics (TOG)*, 28(3):1–8, 2009.
- [60] J. Xu and L. Zikatanov. Some observations on babuška and brezzi theories. *Numerische Mathematik*, 94(1):195–202, 2003.
- [61] M. Yano. Discontinuous galerkin reduced basis empirical quadrature procedure for model reduction of parametrized nonlinear conservation laws. *Advances in Computational Mathematics*, 45(5):2287–2320, 2019.
- [62] M. Yano. Model reduction in computational aerodynamics. *Handbook on Model Order Reduction. Volume 3: Applications. De Gruyter*, pages 201–236, 2021.
- [63] M. Yano and A. T. Patera. An LP empirical quadrature procedure for reduced basis treatment of parametrized nonlinear PDEs. *Computer Methods in Applied Mechanics and Engineering*, 344:1104–1123, 2019.